The histone chaperone CAF-1 maintains the stability of the ribosomal RNA gene cluster by suppressing end resection of replication-associated DNA double-strand breaks.

Hajime Futami[1,2], Mariko Sasaki[1,2,3,4,6,*] and Takehiko Kobayashi[1,2,5,*]

[1]Laboratory of Genome Regeneration, Institute for Quantitative Biosciences (IQB), The University of Tokyo, 1-1-1 Yayoi, Bunkyo-ku, Tokyo 113-0032, Japan
[2]Department of Biological Sciences, Graduate School of Science, The University of Tokyo, 7-3-1 Hongo, Bunkyo-ku, Tokyo 113-0033, Japan
[3]Laboratory of Gene Quantity Biology, Center for Frontier Research, National Institute of Genetics, 1111 Yata, Mishima, Shizuoka 411-8540, Japan
[4]The Graduate University for Advanced Studies, SOKENDAI, 1111 Yata, Mishima, Shizuoka 411-8540, Japan
[5]Collaborative Research Institute for Innovative Microbiology, The University of Tokyo, 1-1-1 Yayoi, Bunkyo-ku, Tokyo 113-0032, Japan

[6]Lead contact: m_sasaki@nig.ac.jp (M.S.)
*Correspondence: tako2015@iqb.u-tokyo.ac.jp (T.K.), m_sasaki@nig.ac.jp (M.S.)

ABSTRACT

In eukaryotes, chromatin assembly is coupled to DNA replication by the histone chaperone chromatin assembly factor-1 (CAF-1). Here, we demonstrate that CAF-1 maintains the stability of the ribosomal RNA gene (rDNA) cluster in budding yeast. Absence of CAF-1 led to homologous recombination (HR)-mediated rDNA copy number changes as well as the production of extrachromosomal rDNA circles in response to Fob1-dependent replication fork arrest at the replication fork barrier (RFB) site in the rDNA. CAF-1-mediated rDNA stabilization depends on its interaction with Proliferating Cell Nuclear Antigen. The absence of CAF-1 affected neither DNA replication fork arrest at the RFB nor subsequent DNA double-strand breaks (DSBs) but led to an increased frequency of DSB end resection, which initiates HR. Absence of CAF-1 caused the derepression of transcription of noncoding RNA from the regulatory promoter E-pro located near the RFB, which contributed to enhanced DSB end resection. Moreover, its absence led to the generation of longer Okazaki fragments, which is indicative of lower nucleosome density in the rDNA. Taken together, our findings suggest that CAF-1-mediated chromatin assembly facilitates silencing of transcription from E-pro and proper nucleosome deposition behind replication forks, leading to the restriction of DSB end resection and subsequent rearrangement-prone DSB repair.

INTRODUCTION

Changes in DNA copy number are introduced by deletion and/or amplification of a DNA segment on the chromosome. DNA copy number changes can alter gene expression levels and compromise cellular integrity, driving tumorigenesis and numerous other diseases [reviewed by (1-4)]. DNA copy number also increases via extrachromosomal circular DNAs that are derived from the chromosome (2,5). Nearly half of cancer cells contain extrachromosomal circular DNAs that carry proto-oncogenes (6), which leads to an increase in their copy number and expression levels, driving the onset and progression of tumorigenesis and drug resistance (2). Thus, understanding the molecular mechanisms underlying chromosomal and extrachromosomal DNA copy number changes is important.

Ribosomal DNA (rDNA) is essential for producing ribosomal RNAs (rRNAs). The budding yeast genome contains ~150 rDNA copies, which are tandemly arrayed at a single locus on Chr XII (Fig. 1A). Each copy contains 35S and 5S rRNA transcription units, which are separated by intergenic spacers containing an origin of DNA replication, a cohesin-associated region (CAR), a replication fork barrier (RFB) sequence and a bidirectional RNA polymerase II (RNAP II) promoter, E-pro, which synthesizes noncoding RNA. Once DNA replication is initiated, the DNA replication fork that progresses in the direction opposite to the 35S rDNA is arrested by the Fob1 protein bound to the RFB site (Fig. 1A) (7-9). The arrested forks are then broken, leading to the formation of one-ended DSBs (10-12). Cells have the mechanisms to maintain their rDNA copy number during DSB repair and when these mechanisms are deficient, cells undergo changes in chromosomal rDNA copy number and the production of extrachromosomal rDNA circles (ERCs) (Fig. 1A) (13-15).

Homologous recombination (HR) is often considered an error-free pathway for repairing two-ended DSBs that are formed in the G2/M phase of the mitotic cell cycle and in meiosis [reviewed by (16,17)]. To repair DSBs by HR, 5'-ended strands of the DSB ends are degraded by a process called DSB end resection [reviewed in (18,19)]. Resected DSBs are subsequently repaired using a homologous sequence on the sister chromatid as a template for Rad52-dependent recombination reactions, which properly restore the original sequence at the DSB site. When DSBs are formed in repetitive regions, however, HR can use a homologous template located at a misaligned position on the sister chromatid or elsewhere in the genome, resulting in chromosome rearrangements [reviewed by (3)].

We previously demonstrated that DSB end resection is normally suppressed for DSBs formed at arrested replication forks at the rDNA RFB, and the repair of these DSBs can be completed without Rad52, an essential factor in HR (20). The replisome component Ctf4 suppresses DSB end resection, and its absence induces HR-dependent DSB repair and rDNA hyperamplification (20). Sir2 is also involved in suppression of DSB end resection (21). However, unlike Ctf4, Sir2 carries out this function by repressing transcription from E-pro (21). Cohesins that keep sister chromatids in close proximity are recruited to the CAR and RFB regions (Fig. 1A) (11,21-23) and are suggested to facilitate the use of the rDNA copy at an aligned position for DSB repair (11,22). The absence of Sir2 and subsequent transcriptional activation lead to the inhibition of cohesin associations with CAR and RFB and rDNA

instability (11,21,22). Therefore, the repression of transcription from E-pro is important for maintaining rDNA stability not only by suppressing DSB end resection and subsequent HR-mediated DSB repair but also by ensuring cohesin binding to rDNA (Fig. 1A).

Eukaryotic organisms must faithfully replicate not only their genetic information but also their chromatin states to maintain genome integrity and epigenetic information. During DNA replication, nucleosomes are disassembled to allow the progression of DNA replication forks [reviewed by (24,25)]. Then, the parental histones are recycled and deposited onto the newly replicated DNA. In addition, newly synthesized histones are deposited onto DNA *de novo* by histone chaperones. The histone chaperone Asf1 first binds to the newly synthesized histones H3-H4 and presents them to the Rtt109 acetyltransferase for acetylation at histone H3K56 (26-28). Acetylated H3-H4 is then transferred to other histone chaperones such as CAF-1 and Rtt106. CAF-1, which consists of Cac1, Cac2 and Cac3 in budding yeast, is recruited to the replisome through its interaction with Proliferating Cell Nuclear Antigen (PCNA) and deposit $(H3\text{-}H4)_2$ tetramers onto the newly synthesized DNA (29-31). In budding yeast, mutations in CAF-1 and PCNA compromise gene silencing at telomeres and silent mating type loci (32,33) and silencing of the marker gene inserted in the rDNA (34). During DNA replication *in vivo*, Okazaki fragment synthesis on the lagging strand is interlinked with the chromatin assembly: Okazaki fragments show a size distribution similar to that of the nucleosome repeat; Okazaki fragment termini are located near nucleosome midpoints (35). CAF-1 facilitates the generation of properly sized Okazaki fragments by mediating nucleosome deposition behind replication forks (35-37).

Here, we showed that the histone chaperone CAF-1 is important for the maintenance of rDNA stability in budding yeast. The absence of CAF-1 led to chromosomal rDNA copy number changes as well as the production of ERCs in a manner dependent on Fob1 and the essential HR factor Rad52. Mutations that compromise the interaction of CAF-1 with PCNA led to rDNA instability. CAF-1 deficiency led to derepression of transcription from E-pro, which is known to cause rDNA instability by inducing DSB end resection at the RFB and inhibiting cohesin associations with rDNA. Indeed, the absence of CAF-1 led to enhanced DSB end resection, although it did not affect the frequency of DNA replication fork arrest at the RFB or subsequent DSB formation. Unexpectedly, its absence did not compromise cohesin binding to the rDNA. Cells lacking CAF-1 showed longer Okazaki fragments in the rDNA, indicating that the nucleosome density decreased in the absence of CAF-1. Taken together, these findings suggest that CAF-1 suppresses DSB end resection and HR-mediated rDNA instability by repressing noncoding RNA transcription from E-pro and facilitating proper chromatin assembly coupled to DNA replication.

Materials and Methods

Yeast Strains and Culture Methods

Yeast strains used in this study are derivatives of W303 (*MATa ade2-1 ura3-1 his3-11, 15 trp1-1 leu2-3,112 can1-100*) and are listed in Table S1. Gene deletion was performed by standard one-step gene replacement methods, followed by confirmation of genotypes by PCR. Alternatively, diploids

heterozygous for gene deletions of interest were constructed and subjected to sporulation, followed by isolation of haploid clones by tetrad dissection. Yeast cells were grown in YPD media (1% w/v yeast extract, 2% w/v peptone, and 2% w/v glucose), except for the experiments in Fig. 2, where cells were grown in SC-Trp media. Five mL of appropriate liquid media was inoculated with a single colony and grown overnight at 30°C. For PFGE and ERC analyses, cultures were collected (5×10^7 cells/plug) and washed twice with 50 mM EDTA (pH 7.5). For two-dimensional (2D) agarose gel electrophoresis, overnight cultures were diluted in 50 mL of YPD medium to an $OD_{600} = 0.1$ and grown until $OD_{600} = 0.4$. The cultures were immediately treated with 1/100 vol of 10% sodium azide, collected (5×10^7 cells/plug), and washed twice with 50 mM EDTA pH 7.5. To prepare RNA, overnight cultures were diluted in 15 mL of YPAD medium (YPD containing 40 µg/mL adenine sulfate) to an $OD_{600} = 0.1$ and collected when the cultures reached an OD_{600} of 0.8. For chromatin immunoprecipitation, overnight cultures of MSY674, 700 and 710 were diluted in 100 mL of YPD medium to an $OD_{600} = 0.2$ and grown until $OD_{600} = 0.8$.

For DSB analyses, time course experiments were performed with MSY360, 937 and 1261, as described previously (20,38). The *GAL-FOB1* strains were grown overnight in YPD media at 30°C. The cells were inoculated into ~200 mL of YP media supplemented with 2% raffinose and one drop of antifoam 204 (Sigma) at an appropriate density to reach ~1×10^7 cells/mL the following morning and subsequently grown overnight at 23°C. To arrest the cells in the G1 phase of the cell cycle, α-factor (ZYMO RESEARCH) was added to the cultures at a final concentration of 20 nM. The cells were incubated at 23°C for 3–4 hrs until >80% of the cells were arrested in G1. Then, 20% galactose was added at a final concentration of 2% to induce *FOB1* expression and the cultures were further incubated for 30 min at 23°C. The cells were collected by centrifugation for 5 min at 4°C at 4,500 × *g*, washed twice with YP medium containing 2% galactose, and resuspended at ~1×10^7 cells/mL in fresh YP medium containing 2% galactose, 0.075 mg/mL pronase E (Sigma) and one drop of antifoam 204 (Sigma). The cells were incubated at 23°C and 10 mL of culture was collected at various time points.

For analysis of Okazaki fragments, we used MSY613, which was constructed from yIW310 that is a kind gift of Iestyn Whitehouse, and MSY1599. We grew the cells in YPD media overnight at 30°C. Overnight cultures were diluted in 200 mL of YPD medium to $OD_{600} = 0.1$ and grown until $OD_{600} = 0.4$. Cultures were divided into two flasks. Doxycycline (100 mg/mL) dissolved in DMSO was added to one culture at a final concentration of 40 µg/mL, and the same volume of DMSO was added to the other culture. These cultures were incubated for 2.5 hrs at 30°C, after which cells were collected. Cells were subsequently washed twice with 50 mM EDTA (pH 8.0).

Plasmid construction

YCplac22 that carries *CAC1* was constructed by the Gibson assembly method as follows. The genomic regions containing the *CAC1* open reading frame and ~500 bp upstream and downstream were amplified by PCR from the *S. cerevisiae* WT strain of the W303 background. Linearized YCplac22 was generated by PCR from YCplac22. These PCR fragments had short homology at each

end and were fused using the Gibsom Assembly according to the manufacturer's instructions. YCplac22 plasmids that carry the *cac1-20* mutant allele were constructed using the PrimeSTAR Mutagenesis Basal Kit (TaKaRa) according to the manufacturer's instructions. Plasmid DNA was sequenced to confirm that the mutations were properly introduced. Primer sequences are available upon request. Plasmids carrying *POL30* (pBL230-0) and the mutant alleles *pol30-6* (pBL230-6), *pol30-8* (pBL230-8) and *pol30-79* (pBL230-79) were kind gifts from Peter Burgers.

Genomic DNA preparation

For PFGE, ERC, DSB, and 2D gel analyses, genomic DNA was prepared in low melting temperature agarose plugs as described previously (20,38). Briefly, collected cells were resuspended in 50 mM EDTA pH 7.5 (33 µL per 5 × 10^7 cells) and incubated at 42°C. For each plug, 33 µL cell suspension was mixed with 66 µL of solution 1 (0.83% low-melting-point agarose SeaPlaque GTG (Lonza), 170 mM sorbitol, 17 mM sodium citrate, 10 mM EDTA (pH 7.5), 0.85% β-mercaptoethanol, and 0.17 mg/mL Zymolyase 100 T (Nacalai)), poured into a plug mold (Bio-Rad) and placed at 4°C for the agarose to be solidified. Plugs were transferred to a 2 mL-tube containing solution 2 (450 mM EDTA pH 7.5, 10 mM Tris-HCl pH 7.5, 7.5% β-mercaptoethanol and 10 µg/mL RNaseA (Macherey-Nagel)) and incubated for 1 hr at 37°C. Plugs were then incubated overnight at 50°C in solution 3 (250 mM EDTA pH 7.5, 10 mM Tris-HCl pH 7.5, 1% sodium dodecyl sulfate (SDS) and 1 mg/mL proteinase K (Nacalai)). Plugs were subsequently washed four times with 50 mM EDTA (pH 7.5) and stored at 4°C in 50 mM EDTA (pH 7.5).

For analysis of Okazaki fragments, genomic DNA was isolated as described previously (35), with slight modifications. Briefly, the cells were washed twice with with lysis buffer (50 mM Tris-HCl [pH 8.0], 50 mM EDTA [pH 8.0], 100 mM NaCl, and 1.5% SDS). Cells were resuspended in 900 µL of SCE solution (1 M sorbitol, 0.1 M sodium citrate, 0.06 M EDTA [pH 7.5]) supplemented with 35 µL of β-mercaptoethanol and 100 µl of 50 mg/mL Zymolyase and mixed by vortexing. The cell suspension was incubated for 3 min at room temperature. The spheroplasts were collected by centrifugation for 5 min at 4,500 × *g*. Spheroplasts were rinsed with 1 mL of SCE and collected by centrifugation for 5 min at 4,500 × *g*. Spheroplasts were resuspended in 500 µL of lysis buffer (50 mM EDTA (pH 8.0), 50 mM Tris-HCl (pH 8.0), 0.5% sodium dodecyl sulfate, and 200 µg/mL proteinase K) and incubated for 2 hrs at 42°C. Proteins were precipitated by adding 200 µL of 5 M potassium acetate and incubating for 5 min on ice, followed by centrifugation at 15,000 rpm for 15 min at 4°C. DNA in the supernatant was precipitated with isopropanol and suspended in 250 µL of STE (10 mM Tris-HCl [pH 8.0], 1 mM EDTA [pH 8.0], 100 mM NaCl containing 80 µg/mL RNaseA [Macherey-Nagel]). RNA was digested by incubation for 1 hr at 37°C. DNA was ethanol precipitated and suspended in 50 µL of TE. The concentration of DNA was quantified by the Qubit Fluorometer.

PFGE

PFGE was performed as described previously (20,38). Briefly, one-third of a plug was placed on a tooth of the comb, including a piece with *Hansenula wingei* chromosomal DNA markers (Bio-Rad). The comb was placed in a gel tray, and 1.0% agarose solution (Pulsed Field Certified Agarose, Bio-Rad) in 0.5× TBE (44.5 mM Tris base, 44.5 mM boric acid and 1 mM EDTA pH 8.0) was poured. PFGE was performed on a Bio-Rad CHEF Mapper XA Chiller System in 2.2 L of 0.5× TBE under the following conditions: 3.0 V/cm for 68 hrs at 14°C, 120° included angle, an initial switch time of 300 s, and a final switch time of 900 s. After electrophoresis, DNA was stained with 0.5 µg/mL EtBr for 30 min, washed with dH_2O for 30 min, and then photographed.

Southern blotting

Agarose gel electrophoresis

ERC assay. The ERC assay was performed as described previously (38,39). Half of the agarose plug was placed on the tooth of the comb. After the comb was set in the gel tray (15 × 25 cm), 300 mL of 0.4% agarose (SeaKem LE Agarose, Lonza) in 1× TAE (40 mM Tris base, 20 mM acetic acid, and 1 mM EDTA pH 8.0) was poured into the tray and allowed to set, after which 500 ng of lambda HindIII DNA marker was applied to an empty lane. The electrophoresis was performed on a Sub-cell GT electrophoresis system (Bio-Rad) in 1.5 L of 1× TAE at 1.0 V/cm for ~48 hrs at 4°C with buffer circulation. The buffer was changed every ~24 hrs. DNA was stained with 0.5 µg/mL ethidium bromide (EtBr) for 30 min and then photographed.

2D gel electrophoresis. 2D gel electrophoresis was performed as described previously with slight modifications (39). One-half of an agarose plug was placed in a 2-mL tube. The plug was equilibrated twice in 1 mL of 1× M buffer (TaKaRa) by rotating the tube for 30 min at room temperature. After discarding the buffer, the plug was incubated in 160 µL of 1× M buffer containing 160 units of NheI (TaKaRa) overnight at 37°C. The plug was placed on the tooth of the comb. The comb was placed in a gel tray (15 × 25 cm), 0.4% agarose solution in 1× TBE was added and the gel was allowed to solidify. A total of 600 ng of lambda HindIII DNA marker was applied to the empty lane. The electrophoresis was performed on a Sub-cell GT electrophoresis system (Bio-Rad) in 1.5 L of 1× TBE at 1.32 V/cm for 14 hrs at room temperature with buffer circulation.

After electrophoresis, DNA was stained with 0.3 µg/mL EtBr for 30 min and then photographed. Gel slices containing DNA ranging from 4.7 to 9.4 kb were excised, rotated 90°, and placed onto the gel tray used for the second agarose gel electrophoresis for which 1.2% agarose solution in 1× TBE containing 0.3 µg/mL of EtBr was poured into the tray. Second-dimension electrophoresis was performed on a Sub-cell GT electrophoresis system (Bio-Rad) in 1.5 L of 1× TBE containing 0.3 µg/mL of EtBr at 6.0 V/cm for 6 hrs at 4°C with buffer circulation. After electrophoresis, the DNA was photographed.

DSB assay. The DSB assay was performed as described previously (Sasaki and Kobayashi, 2017; 2021). One-third of an agarose plug was cut and placed in a 2-mL tube. The plug was

equilibrated four times in 1 mL of 1× TE (10 mM Tris base, pH 7.5 and 1 mM EDTA, pH 8.0) by rotating the tube for 15 min at room temperature. The plug was equilibrated twice in 1 mL of 1× NEBuffer 3.1 (New England Biolabs) by rotating the tube for 30 min at room temperature. After discarding the buffer, the plug was incubated in 160 µL of 1× NEBuffer 3.1 buffer containing 160 units of Bgl II (New England Biolabs) overnight at 37°C. The plug was placed on a tooth of the comb which was set into the gel tray (15 × 25 cm), into which 0.7% agarose solution in 1× TBE was poured; after setting of the gel, 600 ng of lambda BstEII DNA markers were applied to an empty lane. The electrophoresis was performed on a Sub-cell GT electrophoresis system (Bio-Rad) in 1.5 L of 1× TBE at 2.0 V/cm for 22 hrs at room temperature with buffer circulation. After electrophoresis, the DNA was stained with 0.5 µg/mL EtBr for 30 min and then photographed.

Okazaki fragment assay. DNA samples were prepared in 20 µl containing 500 ng of genomic DNA, 2 µL of 10× alkaline buffer (0.5 M NaOH, 10 mM EDTA [pH 8.0]), 2 µl of 0.1% bromophenol blue and 1 µl of 50% glycerol, which were heat-denatured for 5 min at 70°C, followed by rapid chilling on ice. A total of 500 ng of 100 bp DNA ladder was denatured and prepared in parallel. The agarose solution was prepared by dissolving 2.5 g of Seakem LE agarose (Lonza) in 225 mL of Milli-Q water by microwave, followed by cooling to 50°C. Then, 25 mL of 10× alkaline buffer was added to the agarose solution, mixed, poured into a gel tray (15 × 20 cm) in a cold room, and left until the gel solidified. The comb was removed, and 1.45 L of 1× alkaline buffer was added. DNA samples were loaded. The gel was run overnight for 4 hrs at 4°C at 80 V.

DNA transfer

After agarose gel electrophoresis, the gel was incubated by gentle shaking in 500 mL of 0.25 N HCl for 30 min, 500 mL of denaturation solution (0.5 N NaOH, 1.5 M NaCl) for 30 min, and 500 mL of transfer buffer (0.25 N NaOH, 1.5 M NaCl) for 30 min. DNA was transferred to Hybond-XL (GE Healthcare) by the standard capillary transfer method with transfer buffer. DNA was fixed to the membrane by soaking the membrane in 300 mL of freshly prepared 0.4 N NaOH for 10 min with gentle shaking, followed by rinsing the membrane with 2× SSC for 10 min. The membrane was subsequently dried and stored at 4°C.

Probe preparation

Probes were prepared as described previously (20,38). Double-stranded DNA fragments were amplified by PCR. Probe 1 used for ERC, 2D and Okazaki fragment analyses was amplified with the primers 5'-CATTTCCTATAGTTAACAGGACATGCC and 5'-AATTCGCACTATCCAGCTGCACTC, and probe 2 used for DSB analysis was amplified with the primers 5'-ACGAACGACAAGCCTACTCG and 5'-AAAAGGTGCGGAAATGGCTG. A portion of the PCR products was gel-purified and seeded for a second round of PCR with the same primers. The PCR products were gel-purified and 50 ng was used for random priming reactions in the presence of the radiolabeled nucleotide, [α-^{32}P]-dCTP (3,000 Ci/mmol, 10 mCi/mL, Perkin Elmer), using Random Primer DNA Labeling Kit (TaKaRa), according to the manufacturer's instructions. Unincorporated nucleotides were removed using ProbeQuant G-50 Micro Columns (GE Healthcare). The radiolabeled probes were heat-denatured for 5 min at 100°C, immediately prior to hybridization to the membrane.

Hybridization

Southern hybridization was performed as described previously (20,38). The membrane was prewetted with 0.5 M phosphate buffer pH 7.2 and prehybridized for 1 hr at 65°C with 25 mL of hybridization buffer (1% bovine serum albumin, 0.5 M phosphate buffer, pH 7.2, 7% SDS, 1 mM EDTA pH 8.0). After the buffer was discarded, the membrane was hybridized with 25 mL of hybridization buffer and heat-denatured probe overnight at 65°C. The membrane was washed four times for 15 min at 65°C with wash buffer (40 mM phosphate buffer pH 7.2, 1% SDS, 1 mM EDTA pH 8.0) and exposed to a phosphor screen.

Image analysis

Membranes were exposed to a phosphor screen for several days to achieve a high signal-to-noise ratio for DNA molecules that are low in abundance, such as ERCs, replication intermediates in 2D assays, and arrested forks and DSBs. The radioactive signal was detected using a Typhoon FLA 7000 (GE Healthcare). In the ERC assays, the genomic rDNA signal was used for normalization of the ERC signals. Thus, the membranes were re-exposed to the phosphor screen for a short time before this signal reached saturation. ERC bands and genomic rDNA were quantified using FUJIFILM Multi Gauge version 2.0 software (Fujifilm) and scans from long and short exposures, respectively. The levels of ERCs were calculated by dividing the sum of the signal intensities of the ERCs by those of the genomic rDNA. When the levels of ERCs were compared between samples loaded on different gels, pieces of the plug excised from a specific DNA sample were loaded on different gels, blotted and hybridized. The signals of these plugs were used for normalization of samples on different gels. In 2D analyses, bubbles, Y arcs, RFB spots, X and double Y spots were quantified using ImageJ (NIH). The RFB activity was calculated as the ratio between the signal for the spot with arrested forks and the sum of signals encompassing the total DNA replication and recombination intermediates. The signals of DSBs and arrested forks were quantified using FUJIFILM Multi Gauge version 2.0 software (Fujifilm). The frequency of DSBs was calculated by normalizing the DSB signal to that of the arrested forks.

Yeast RNA preparation

RNA was prepared as described previously (40), with slight modifications. The collected cells were resuspended in 400 µL of TES (10 mM Tris-HCl pH 7.5, 10 mM EDTA pH 7.5, 0.5% SDS) and 400 µL of acidic phenol by vortexing for approximately 10 s. Cells were incubated at 65°C for 1 hr with occasional vortexing every 15 min. The cell suspensions were incubated for 5 min on ice and centrifuged at 20,000 × *g* for 10 min at 4°C. The aqueous phase was transferred to a new tube and mixed with an equal volume of acidic phenol by vortexing for 10 s. Samples were incubated for 5 min on ice and centrifuged at 20,000 × *g* for 10 min at 4°C. The aqueous phase was transferred to a new tube. Then, 1/10 vol. of 3 M sodium acetate (pH 5.3) and 2.5 vol. of 100% ethanol were added and RNA was precipitated overnight at -20°C. After centrifugation at 20,000 × *g* for 10 min at 4°C, RNA was washed with 70% ethanol. The RNA pellets were resuspended in 30 µL of dH_2O treated with

0.1% diethylpyrocarbonate (DEPC). The concentration of RNA was quantified using a NanoDrop ND-1000 spectrophotometer (Thermo Fisher Scientific). RNA samples were stored at -80°C.

Northern blotting

Thirty µg of total RNA was brought up to 7 µL with DEPC-treated dH_2O and mixed with 17 µL of RNA sample buffer (396 µL of deionized formamide, 120 µL of 10× MOPS buffer [0.2 M MOPS, 50 mM sodium acetate pH 5.2, 10 mM EDTA pH 7.5 in DEPC-treated dH_2O], and 162 µL of 37% formaldehyde). A total of 1.8 µg of DynaMarker RNA High Markers (BioDynamics Laboratory) were brought up to 4.8 µL with DEPC-treated dH_2O and mixed with 11.2 µL of RNA sample buffer. The samples were heated at 65°C for 20 min, followed by rapid chilling on ice. To the samples and size markers, 6 and 4 µL of 6× Gel Loading Dye (B7025S, New England Biolabs) and 1.5 and 1 µL of 2.5 mg/mL EtBr were added. Two 1% agarose gels were made by dissolving 1 g of agarose powder in 73 mL of DEPC-treated dH_2O, and, after cooling to 60°C, 17 mL of 37% formaldehyde and 10 mL of 10× MOPS buffer were added. The solution was poured into a gel tray (13 × 12 cm) and allowed to set. Agarose gel electrophoresis on a Mupid EX system (Takara) was performed in 400 mL of 1× MOPS buffer at 20 V for 20 min and then at 100 V until the bromophenol blue dye migrated approximately 2/3 of the gel. After electrophoresis, the gel was photographed and RNA was transferred to Hybond-N+ (GE Healthcare) by standard capillary transfer.

Strand-specific probes were prepared from double-stranded DNA fragments, amplified by PCR and gel-purified. The PCR primers used for probe 3 (against IGS1-R, IGS2-R), 5'-TCGCCAACCATTCCATATCT and 5'-CGATGAGGATGATAGTGTGTAAGA; for probe 4 (against IGS1-F) were 5'-AGGGAAATGGAGGGAAGAGA and 5'-TCTTGGCTTCCTATGCTAAATCC, and for detecting TSA1, 5′-CAAGTTCAAAAGCAAGCTCC and 5′-ACCAATCTCAAGGCTTCGTC. Strand-specific probes were then prepared by linear PCR in a final volume of 20 µL containing 0.2 mM dATP, 0.2 mM dTTP, 0.2 mM dGTP, 50 µL [α-^{32}P]-dCTP (3,000 Ci/mmol, 10 mCi/mL, Perkin Elmer), 1.25 units ExTaq (TaKaRa), 1× ExTaq buffer, 50 ng of PCR product as a template, and 10 µM primer (5'-AGTTCCAGAGAGGCAGCGTA for probe 3, 5'-CATTATGCTCATTGGGTTGC for probe 4). PCR was initiated by a denaturation step at 94°C for 3 min, followed by 35 cycles of amplification (96°C for 20 s, 51°C for 20 s, and 72°C for 30 s), and a final step at 72°C for 3 min. Unincorporated nucleotides were removed using ProbeQuant G-50 Micro Columns (GE Healthcare). The radiolabeled probes were heat denatured by incubating for 5 min at 100°C, immediately prior to hybridization to the membrane.

The membrane was incubated with 10 mL of ULTRAhyb Ultrasensitive Hybridization Buffer (Thermo Fisher) at 42°C for 1 h. The heat-denatured probe was incubated with the membrane overnight at 42°C. The membrane was rinsed twice with 2× SSC, washed for 15 min at 42°C twice with wash buffer 1 (2× SSC, 0.1% SDS), and washed for 15 min at 42°C twice with wash buffer 2 (0.1× SSC, 0.1% SDS). The membrane was exposed to phosphor screens for several days, and radioactive signals were detected using a Typhoon FLA 7000 (GE Healthcare). Probes were stripped by incubating the membrane with boiled 0.1% SDS by shaking for ~30 min, rinsed with 2× SSC, and

rehybridized with the TSA1 probe that was prepared as described above. Signals of IGS-F, IGS1-R, IGS2-R, and TSA1 were quantified using FUJIFILM Multi Gauge version 2.0 software (Fujifilm). The levels of IGS transcripts were normalized to the TSA1 signal.

Chromatin immunoprecipitation-quantitative PCR analysis

Thirty-five millilitres of cultures were transferred to 50 mL conical tubes, to which 972 μL of 37% formaldehyde was added at a final concentration of 1%, and the cells were crosslinked by shaking for 30 min at room temperature on a reciprocal shaker at 60 r/min. The crosslinking reaction was quenched by adding glycine to a final concentration of 125 mM and shaking for 5 min at room temperature on a reciprocal shaker at 60 r/min. The cells were collected by centrifugation at 2,380 × *g* for 3 min at 4°C, washed twice with 20 mL of TBS (20 mM Tris, 150 mM NaCl, pH 7.4), and washed once with 5 mL of FA lysis buffer (50 mM HEPES-KOH, pH 7.4; 150 mM NaCl; 1 mM EDTA, pH 8.0; 1% Triton X-100; 0.1% sodium deoxycholate; 0.1% SDS). The cell pellets were resuspended in 0.5 mL of FA lysis buffer, transferred to a 1.5 mL microtube, and collected by centrifugation at 2,380 × *g* for 1 min at 4°C.

The cells were resuspended in 400 μL of FA lysis buffer supplemented with 1 mM PMSF and 1× Complete EDTA-free solution and transferred to a 2 mL tube (STC-0250, Yasui Kikai). Zirconia/silica beads (1.5 g) 0.5 mm in diameter were added to each tube. The cells were disrupted using a Multibead Shocker (Yasui Kikai) for 20 cycles of 30 sec on at 2,700 rpm and 30 sec off at 2°C. A burned 23–26-G needle was used to make a few holes at the bottom of the tube, which was inserted into a 5 mL tube and centrifuged at 1,000 × *g* for 30 sec at 4°C. The cell lysate was transferred to a 1.5 mL TPX tube. Chromatin was sheared by sonication at 4°C at high power with ice on a Bioruptor for three sets of 5 cycles of 30 sec on and 30 sec off. Sheared chromatin samples were centrifuged at 20,380 × *g* for 15 min at 4°C and recovered with the same volume of FA lysis buffer. A total of 10 μL was set aside as input DNA.

A total of 320 μL was transferred to a low-binding tube (Costar) and incubated with 10 μL of Dynabeads Protein G (Thermo Fisher) for 1 hr at 4°C, after which the precleared samples were transferred to a new low-binding tube. Then, 2.1 μg of anti-Flag antibody (M2; Sigma-Aldrich) was added to each tube, and the mixture was incubated for 3 hrs at 4°C. The chromatin samples were incubated with an antibody and then incubated overnight at 4°C with 12 μL of Dynabeads Protein G, which was preincubated with 5 mg/mL BSA solution in PBS. The beads were washed twice with 0.5 mL of FA lysis buffer, twice with 0.5 mL of FA lysis buffer supplemented with 360 mM NaCl, twice with 0.5 ml of ChIP wash buffer (10 mM Tris-HCl (pH 8.0), 250 mM lithium chloride, 1 mM EDTA (pH 8.0), 0.5% NP-40 and 0.5% sodium deoxycholate), and twice with 0.5 mL of 1× TE buffer. After the buffer was completely removed, 54 μL of ChIP elution buffer (50 mM Tris-HCl (pH 8.0), 10 mM EDTA, and 1% SDS) was added, and the immunoprecipitates were eluted from the beads by incubating for 15 min at 65°C. Fifty μL of eluate was transferred to a new tube and mixed with 150 μL of TE containing 1% SDS. Ten μL of input sample was mixed with 190 μL of TE containing 1%. To each sample,

RNaseA was added at a final concentration of 50 μg/mL. These samples were incubated overnight at 65°C for reverse crosslinking and RNA digestion. Then, proteinase K was added at a final concentration of 0.75 mg/mL, and the mixture was incubated for 2 hrs at 50°C. DNA was purified using a QIAquick PCR Purification Kit (QIAGEN). DNA was eluted with 100 μL of dH_2O.

qPCR was performed on a Thermal Cycler Dice Real Time System II (TaKaRa) with THUNDERBIRD SYBR qPCR Mix or Next SYBR qPCR Mix (TOYOBO) according to the manufacturers' instructions. One of the input samples was diluted serially to 1/20, 1/200, 1/2,000 and 1/20,000 dilutions, which were subsequently used to construct the standard curve. All the input samples were subsequently diluted 400-fold. IP samples were diluted 10-fold. qPCR was performed with all the diluted samples as well as the standard. The amount of DNA in each sample was subsequently determined relative to the standard. After considering dilution factors, % input was expressed for each time point of each culture as the amount of DNA in the IP relative to that in the input.

Quantification and statistical analysis

Statistical analyses were performed using GraphPad Prism, as described in figure legends.

RESULTS

CAF-1 is required for the maintenance of rDNA stability.

To test whether Cac1, Cac2 and Cac3 function as a complex in the maintenance of rDNA stability, we first compared the degree of rDNA instability in *cac1Δ*, *cac2Δ*, and *cac3Δ* single mutants. To this end, we isolated genomic DNA from these mutants, separated DNA by pulsed-field gel electrophoresis (PFGE), and examined the size heterogeneity of chr XII carrying the rDNA array. The wild-type (WT) strain showed a homogeneous chr XII band, but all the single *caf-1* mutants showed extremely smeared bands to the degree similar to that seen for the *sir2Δ* mutant (Fig. 1B). Therefore, the absence of the subunits of CAF-1 induced chromosomal rDNA instability, consistent with a previous finding (41).

We next analyzed ERCs that can be produced during chromosomal rDNA copy number changes (11,42). The levels of ERCs in the *cac1Δ* and *cac2Δ* single mutants were ~3-fold greater than those in the WT strain and their levels were comparable to that detected in the *sir2Δ* mutant (Fig. 1C, 1D). The *cac3Δ* mutant showed less severe rDNA instability than the *cac1Δ* and *cac2Δ* mutants but still showed an ~1.7-fold increase in the ERC level, compared to that of the WT strain (Fig. 1C, 1D). Although monomeric ERCs were predominant in the WT, the *caf-1* mutants produced more dimeric and multimeric ERCs (Fig. 1E). In both PFGE and ERC analyses, the phenotypes of the double and triple *caf-1* mutants were similar to those of the *cac1Δ* and *cac2Δ* single mutants (Fig. 1C, 1D). Therefore, Cac1, Cac2 and Cac3 function as a complex to stabilize rDNA by suppressing chromosomal rDNA copy number changes and the production of ERCs, especially multimeric ERCs.

The interaction of CAF-1 with PCNA is critical for rDNA stabilization.

CAF-1 is known to be recruited by the interaction with PCNA and deposit histones onto the newly synthesized DNA (29-31). To test whether the recruitment by PCNA is important for the function of CAF-1 in rDNA, we examined the effects of mutations that compromise the interaction between CAF-1 and PCNA. To this end, we introduced an empty plasmid or plasmids that carry the *CAC1* or *cac1-20* allele that had a mutation in the PCNA-binding motif in the Cac1 protein (43) and analyzed rDNA stability by PFGE and ERC analyses. The *cac1Δ* mutant transformed with an empty vector showed smeared chr XII bands, while the *cac1Δ* mutant complemented with a plasmid carrying *CAC1* showed sharp bands (Fig. 2A). Expression of *cac1-20* in the *cac1Δ* mutant showed that chr XII bands appeared less smeared than those in the *cac1Δ* mutant with an empty vector, although the bands were still more smeared than those in the *cac1Δ* mutant expressing *CAC1* (Fig. 2A). The level of ERCs was ~2.5-fold greater in the *cac1Δ* mutant with an empty vector, compared to the *cac1Δ* mutant expressing *CAC1* (Fig. 2B, 2C). Expression of *cac1-20* in the *cac1Δ* mutant caused a slight reduction in the level of ERCs, but it was still ~2-fold higher than that in the *cac1Δ* mutant expressing *CAC1* (Fig. 2B, 2C). Thus, the defective PCNA binding of the *cac1* allele did not suppress rDNA instability in the *cac1Δ* mutant.

We also analyzed the effects of three mutations in *POL30* that encodes a PCNA: *pol30-6*, *pol30-8*, and *pol30-79*, which results in a substantial loss of the ability of PCNA to bind to Cac1p (31). Because the *POL30* gene is essential, we constructed a diploid strain heterozygous for *pol30Δ*, transformed the strain with plasmids carrying wild-type *POL30* or mutant alleles, and isolated haploid *pol30Δ* mutants inheriting plasmids by tetrad dissection. In PFGE, the *pol30Δ* mutant complemented with *POL30* showed sharp chr XII bands, but the *pol30Δ* mutants expressing *pol30-6*, *pol30-8* or *pol30-79* showed smeared chr XII bands (Fig. 2D). Moreover, compared with the *pol30Δ* mutant complemented with *POL30*, the *pol30Δ* mutant expressing mutant alleles showed ~2.5-fold or even higher level of ERCs (Fig. 2E, 2F). Taken together, these findings suggest that the interaction of CAF-1 with PCNA, which is necessary for the deposition of histones onto newly synthesized DNA, is important for the maintenance of rDNA stability.

CAF-1 suppresses HR-mediated rDNA instability via an Fob1-dependent pathway.

To understand how CAF-1 maintains rDNA stability, we examined whether rDNA instability in the *cac1Δ* mutant depends on Fob1 and the HR protein Rad52. To this end, we constructed a diploid strain that was heterozygous for *cac1Δ*, *fob1* and rad52Δ, isolated haploid clones by tetrad dissection, and analyzed their rDNA stability by PFGE. The *cac1Δ* mutant showed smeared chr XII bands, but this smearing was suppressed by *fob1*, suggesting that rDNA instability in the *caf-1* mutant depends on Fob1 (Fig. 3A), consistent with previous findings (41). Smearing of the chr XII bands in the *cac1Δ* mutant was also suppressed by *rad52Δ* (Fig. 3A). Furthermore, ERC production in the *cac1Δ* mutant was suppressed by *fob1* and by *rad52Δ* (Fig. 3B, 3C). Thus, CAF-1 suppresses Rad52-dependent rDNA copy number changes in response to Fob1-dependent replication fork arrest at the RFB.

To understand how CAF-1 functions in the Fob1-dependent pathway, we examined the pattern of DNA replication and recombination in the rDNA region in the *cac1Δ* mutant. We isolated genomic DNA from exponentially growing WT and *cac1Δ* cells, digested it with the restriction enzyme NheI, which has two recognition sites within each rDNA copy (Fig. 3D), and performed two-dimensional (2D) agarose gel electrophoresis to separates replication and recombination intermediates (44). DNA was first separated by agarose gel electrophoresis according to molecular mass in the first dimension and then according to molecular mass and shape in the second dimension, followed by Southern blotting with the rDNA probe 1 (Fig. 3D). DNA molecules where DNA replication is initiated from a replication origin are detected as bubble-shaped molecules, while DNA molecules where replication progresses passively through the NheI fragment generate a Y arc (Fig. 3E). DNA replication forks that are arrested at the RFB produce an intense signal along the Y arc (Fig. 3E). The frequency of replication initiation in the *cac1Δ* mutant appeared lower than that in the WT, but this difference was not statistically significant (Fig. 3F). The frequency of replication fork arrest at RFB was comparable between the WT and *cac1Δ* mutant strains (Fig. 3G). X-shaped molecules that protrude from the 2N spot include recombination intermediates, while double-Y molecules correspond to arrested fork intermediates to which the converging fork arrives from a downstream DNA replication origin (Fig. 3E). The levels of these molecules in the *cac1Δ* mutant were similar to those in the WT (Fig. 3H). Therefore, these findings suggest that CAF-1 does not affect replication patterns in the rDNA, raising the possibility that CAF-1 affects DSB formation or repair rather than DNA replication patterns in the rDNA.

The CAF-1-mediated repression of E-pro is important for rDNA stabilization.

CAF-1 is involved not only in gene silencing at telomeres and silent mating type loci but also in silencing of the marker genes inserted in rDNA (31,34,45). Therefore, we next examined whether CAF-1 is involved in the regulation of transcription from the native noncoding RNA promoter E-pro. We extracted total RNA from WT, *cac1Δ*, *cac2Δ* and *cac3Δ* mutants, separated RNA by agarose gel electrophoresis under denaturing conditions and detected the transcripts from E-pro by Northern blotting with strand-specific probes (Fig. 4A). The *sir2Δ* mutant, in which transcription from E-pro is derepressed (22), was analyzed in parallel. IGS1-R transcripts of ~300–650 nt in size were detected in the *sir2Δ* mutant, consistent with previous findings (46,47), and their level in the *sir2Δ* mutant was ~30-fold greater than that in WT cells (Fig. 4B, 4C). The levels of IGS1-R transcripts was greater in all the *caf-1Δ* mutants than in the WT cells, but their levels were not as high as those seen in the *sir2Δ* mutant (Fig. 4C). IGS1-F transcripts of the size ranging from ~800 to ~1,200 nt were detected in the *sir2Δ* mutant at a level that was >10-fold higher than that in WT cells (Fig. 4D, 4E), consistent with previous findings (46,47). Compared with those in the WT, the level of IGS1-F transcripts in the *caf-1* mutants was greater, but the degree of the increase was less than that in the *sir2Δ* mutant (Fig. 4D, 4E). For both the IGS1-R and IGS1-F transcripts, the *cac1Δ* and *cac2Δ* mutants showed stronger phenotypes than did the *cac3Δ* mutant (Fig. 4B–4E). Taken together, CAF-1 functions to repress transcription from E-pro but its contribution is smaller than that of Sir2.

To directly test the causal relationship between transcription near the RFB site and rDNA instability in the *caf-1* mutant, we used the strain that was engineered to have a galactose-inducible, bi-directional *GAL1/10* promoter in place of E-pro in all the rDNA copies, which is hereafter referred to as the Gal-pro strain (Fig. 4A) (22). Transcription from the *GAL1/10* promoter was maintained at an extremely low level when cells were grown in the presence of raffinose but was induced when galactose was added to the media (Fig. 4F, 4G). When the cells were grown in the presence of raffinose, ERC production was strongly suppressed in both the WT and *sir2Δ* mutant strains in the Gal-pro background (Fig. 4H, 4I). In contrast, in the Gal-pro *cac1Δ* mutant, the level of ERCs was ~4-fold higher than that in the Gal-pro strain even in the presence of raffinose, in which transcription was not detected (Fig. 4H, 4I). This difference was statistically significant according to a t test, although not by multiple comparison tests. Thus, the pathway that is independent of nearby transcription contributes to ERC production in the *cac1Δ* mutant.

The addition of galactose to the media induced ERC production by 8- and 12-fold in the WT and *sir2Δ* mutant strains in the Gal-pro background, respectively (Fig. 4H, 4I). Thus, ERC production in the WT and *sir2Δ* mutant depends on the transcriptional activity near the RFB, consistent with previous findings (Kobayashi and Ganley, 2005; Saka et al., 2013). In the *cac1Δ* background, the addition of galactose to the media led to an ~3-fold increase in the level of ERCs, compared to that in *cac1Δ* cells grown in the raffinose-containing media (Fig. 4H, 4I). Thus, the transcriptional activity near the RFB induced ERC production in the *cac1Δ* background, but the degree of its induction was lower than that in the WT and *sir2Δ* cells. Taken together, these findings suggest that CAF-1 stabilizes the rDNA in a manner that is both dependent and independent of transcription near the RFB.

CAF-1 suppresses DSB end resection.

To test whether enhanced E-pro activity resulted in the dissociation of cohesin from the CAR, we conducted chromatin immunoprecipitation and quantitative PCR in the WT, *cac1Δ* and *sir2Δ* strains expressing the cohesin subunit Mcd1 tagged with a Flag epitope tag (Fig. 5A). Cohesin was associated with the positive control region near a centromere on chr VI (Fig. 5B) (48) but it was not with the region near *YEL008W* on chr V (Fig. 5C), where cohesin association was not observed in a previous chromatin immunoprecipitation sequencing study (49). In the rDNA region, cohesin was most enriched in the CAR in exponentially growing WT cells, and cohesin association was decreased in the *sir2Δ* mutant (Fig. 5A, ii), consistent with previous findings (11). Although the *cac1Δ* mutant showed enhanced transcription from E-pro, compared to that in WT cells, it did not result in the inhibition of cohesin association with the CAR (Fig. 5A, ii).

Transcription from E-pro also induces end resection of DSBs formed at the RFB (21). To test whether enhanced transcription in the *cac1Δ* mutant induces DSB end resection, we conducted time course experiments during synchronous S phase progression in WT and *cac1Δ* cells that express the *FOB1* gene under the control of the *GAL1* promoter. We prepared genomic DNA, digested DNA with Bgl II, and separated DNA by conventional agarose gel electrophoresis, followed by detection of arrested forks, DSBs, and resected DSBs by Southern blotting (Fig. 5E). Cac1 deficiency did not

affect DSB formation (Fig. 5F). Consistent with previous findings (21), the absence of Sir2 relieved suppression of DSB end resection (Fig. 5G). The absence of Cac1 also caused an ~3-fold increase in the frequency of DSB end resection, compared to that in WT cells (Fig. 5G). Taken together, these findings suggest that CAF-1 prevents HR-mediated rDNA instability by suppressing DSB end resection.

CAF-1-mediated chromatin assembly facilitates properly spaced lagging strand synthesis.

During DNA replication *in vivo*, Okazaki fragment synthesis is interlinked with the chromatin assembly (35). Thus, analysis of Okazaki fragments allows us to assess nucleosome assembly *in vivo*. When unligated Okazaki fragments are analyzed in bulk DNA, the absence of Cac1 severely diminishes the nucleosome-sized periodicity of Okazaki fragments, indicating that longer Okazaki fragments are produced (35-37). To assess Okazaki fragment synthesis in the rDNA region, we used the strains carrying a doxycycline-repressible allele of *CDC9* that encodes a DNA ligase that joins Okazaki fragments, isolated genomic DNA from cultures where *CDC9* was shut off or kept expressed, and separated DNA by agarose gel electrophoresis under denaturing conditions, followed by Southern blotting with an rDNA probe. Upon *CDC9* inhibition, WT cells showed a ladder of bands that appeared to be sized according to the nucleosomal repeat (165 bp) (Fig. 6A). Although the same amount of genomic DNA was analyzed, the abundance of DNA fragments was lower in the *cac1Δ* mutant than in the WT (Fig. 6A). Therefore, in line with previous findings (35-37), the *cac1Δ* mutant had a lower nucleosome density and generated longer Okazaki fragments in the rDNA.

DISCUSSIONS

Eukaryotic organisms have evolved mechanisms that faithfully maintain genetic and epigenetic information. CAF-1 is one of the factors involved in these processes and ensures the coordination of DNA replication with chromatin assembly (50). In this study, we demonstrated that CAF-1 plays a crucial role in maintaining the stability of the rDNA array in response to DNA replication fork arrest by suppressing DSB end resection and subsequent HR-mediated repair (Figs. 1, 3, 4).

The absence of CAF-1 not only caused frequent expansion and contraction of the chromosomal rDNA array but also enhanced ERC production (Fig. 1). Our findings that these rDNA instability phenotypes were suppressed by the introduction of *fob1* and *rad52Δ* mutations suggest that CAF-1 suppresses HR-mediated rDNA instability during the repair of DSBs formed in response to Fob1-dependent DNA replication fork arrest (Fig. 3A–3C). In the *cac1Δ* mutant, DSB end resection, which is required for initiating HR, was enhanced by ~3-fold, compared to that in WT cells (Fig. 5E, 5G). Thus, CAF-1-mediated suppression of DSB end resection is crucial for rDNA stabilization (Fig. 6B).

Extending the previous finding that CAF-1 silences the marker gene integrated into the rDNA (34), it is also involved in silencing noncoding RNA transcription from the endogenous E-pro (Fig. 4B–4E, 6B). The derepression of transcription at the E-pro in the *sir2Δ* mutant decreases cohesin binding to the rDNA (Fig. 4B–4E, Fig. 5A-ii) (11,22). In contrast to these previous findings, the *cac1Δ* mutant,

which showed an ~4-fold increase in the transcription level at the E-pro locus, did not show defective cohesin binding but rather showed a slight increase in cohesin binding to the rDNA (Fig. 4B–4E, 5A-ii). A previous finding demonstrated that the absence of Cac1 leads to increased cohesin association near centromeres and other known cohesin-binding sites outside of the rDNA but does not alter the level of sister chromatid cohesion (51). Our ChIP analysis results support this previous finding for cohesin binding patterns in the *cac1Δ* mutant (Fig. 5A-ii). Although we did not analyze the status of sister chromatid cohesion at the rDNA locus in this study, CAF-1 is less likely to function to regulate cohesin binding and cohesion at the rDNA to stabilize the rDNA.

Using the Gal-pro *cac1Δ* strain, we showed that the rDNA is destabilized in the *cac1Δ* mutant in manners that are both dependent and independent of the transcriptional activity near the RFB (Fig. 4F–4I). We previously demonstrated that this nearby transcription induces DSB end resection at the RFB (21). Thus, derepression of transcription from E-pro in the *cac1Δ* mutant contributes to enhanced DSB end resection in the *cac1Δ* mutant (Fig. 5E, 5G), which induces HR-mediated rDNA instability.

CAF-1 is recruited to the replication fork through its interaction with PCNA, which ensures chromatin assembly onto replicating DNA (29,30,35-37,52). We analyzed Okazaki fragments during rDNA replication to assess chromatin assembly around the RFB and found that abundance of nucleosome-sized Okazaki fragments decreased in the *cac1Δ* mutant (Fig. 6A), indicating that the nucleosome occupancy behind arrested forks and thus around DSBs at the RFB decreases when CAF-1 is absent (Fig. 6B). Thus, we envision that CAF-1 ensures proper nucleosome density on newly replicated DNA, which may be important for preventing DSB end resection enzymes from gaining access to the ends of DSBs formed at the RFB. It needs to be examined in future studies why the Gal-pro *cac1Δ* strain grown in the presence of galactose did not induce ERC production to a degree comparable to that of the WT and *sir2Δ* mutant strains (Fig. 4H, 4I).

The *cac1Δ* mutant showed rDNA instability to a degree comparable to that of the *sir2Δ* mutant (Fig. 1). However, this mutant did not show defects in the steps that are known to affect rDNA stability, such as cohesion binding and DSB end resection, to the degree seen in the *sir2Δ* mutant (Fig. 5). Thus, CAF-1 may have an additional function at a previously unidentified step. CAF-1 loads newly synthesized histones H3-H4, where histone H3K56 is acetylated by the histone chaperone Rtt109 (26-28). Defective acetylation of histone H3K56 renders cells sensitive to DNA damaging agents, suggesting that chromatin with histone H3K56 acetylation facilitates DNA repair (27). We previously demonstrated that the absence of Rtt109, which is responsible for the acetylation of histone H3K56, induces rDNA instability (53). We speculate that during DSB repair, Rad52 preferentially uses a homologous rDNA copy that contains chromatin with acetylated histone H3K56 (Fig. 6B). Deficiency of CAF-1 results in defects in the deposition of nucleosomes with acetylated histone H3K56 on replicating DNA (Fig. 6B, right). The likelihood of having acetylated histone H3K56 is low behind the arrested forks at the RFB. Thus, in cells lacking CAF-1, Rad52 may not use the rDNA copy at an aligned position for DSB repair due to the absence of H3K56 acetylation but instead preferentially uses a copy that is distant from the DSB site, leading to chromosomal rDNA copy number changes and ERC production (Fig. 6B).

DATA AVAILABILITY

All data are available upon request.

FUNDING

M.S.: Grants-in-Aid for Scientific Research (20H05382 and 18H04709), the JST FOREST Program (grant number JPMJFR214P), the Naito Foundation; T.K.: Grants-in-Aid for Scientific Research (17H01443 and 21H04761), JST CREST (grant number JPMJCR19S3), JST AMED (JP21gm1110010).

ACKNOWLEDGEMENTS

We are grateful to Peter Burgers for the plasmids pBL230-0, 6, 8 and 79 and Iestyn Whitehouse for the yIW310 strain. We thank members of the Kobayashi laboratory for discussions.

AUTHOR CONTRIBUTIONS

H.F., M.S. and T.K. designed the experiments, analyzed the data and wrote the paper. H.F. and M.S. performed the experiments.

CONFLICT OF INTEREST STATEMENT

The authors declare no competing interests.

REFERENCES

1. Carvalho, C.M. and Lupski, J.R. (2016) Mechanisms underlying structural variant formation in genomic disorders. *Nat Rev Genet*, **17**, 224-238.

2. Yan, X., Mischel, P. and Chang, H. (2024) Extrachromosomal DNA in cancer. *Nature Reviews Cancer*.

3. Sasaki, M., Lange, J. and Keeney, S. (2010) Genome destabilization by homologous recombination in the germ line. *Nat Rev Mol Cell Biol*, **11**, 182-195.

4. Harel, T. and Lupski, J.R. (2018) Genomic disorders 20 years on-mechanisms for clinical manifestations. *Clin Genet*, **93**, 439-449.

5. Verhaak, R.G.W., Bafna, V. and Mischel, P.S. (2019) Extrachromosomal oncogene amplification in tumour pathogenesis and evolution. *Nat Rev Cancer*, **19**, 283-288.

6. Turner, K.M., Deshpande, V., Beyter, D., Koga, T., Rusert, J., Lee, C., Li, B., Arden, K., Ren, B., Nathanson, D.A. *et al.* (2017) Extrachromosomal oncogene amplification drives tumour evolution and genetic heterogeneity. *Nature*, **543**, 122-125.

7. Brewer, B.J. and Fangman, W.L. (1988) A replication fork barrier at the 3' end of yeast ribosomal RNA genes. *Cell*, **55**, 637-643.

8. Brewer, B.J., Lockshon, D. and Fangman, W.L. (1992) The arrest of replication forks in the rDNA of yeast occurs independently of transcription. *Cell*, **71**, 267-276.

9. Kobayashi, T., Hidaka, M., Nishizawa, M. and Horiuchi, T. (1992) Identification of a site required for DNA replication fork blocking activity in the rRNA gene cluster in Saccharomyces cerevisiae. *Mol Gen Genet*, **233**, 355-362.

10. Burkhalter, M.D. and Sogo, J.M. (2004) rDNA enhancer affects replication initiation and mitotic recombination: Fob1 mediates nucleolytic processing independently of replication. *Molecular cell*, **15**, 409-421.

11. Kobayashi, T., Horiuchi, T., Tongaonkar, P., Vu, L. and Nomura, M. (2004) SIR2 regulates recombination between different rDNA repeats, but not recombination within individual rRNA genes in yeast. *Cell*, **117**, 441-453.

12. Weitao, T., Budd, M., Hoopes, L.L. and Campbell, J.L. (2003) Dna2 helicase/nuclease causes replicative fork stalling and double-strand breaks in the ribosomal DNA of Saccharomyces cerevisiae. *The Journal of biological chemistry*, **278**, 22513-22522.

13. Kobayashi, T. (2011) Regulation of ribosomal RNA gene copy number and its role in modulating genome integrity and evolutionary adaptability in yeast. *Cellular and molecular life sciences : CMLS*, **68**, 1395-1403.

14. Kobayashi, T. and Sasaki, M. (2017) rDNA stability is supported by many "Buffer genes" - Introduction to the Yeast rDNA Stability Database. *FEMS Yeast Res*.

15. Sasaki, M. and Kobayashi, T. (2023) Regulatory processes that maintain or alter ribosomal DNA stability during the repair of programmed DNA double-strand breaks. *Genes Genet Syst*, **98**, 103-119.

16. Paques, F. and Haber, J.E. (1999) Multiple pathways of recombination induced by double-strand breaks in Saccharomyces cerevisiae. *Microbiol Mol Biol Rev*, **63**, 349-404.

17. Symington, L.S., Rothstein, R. and Lisby, M. (2014) Mechanisms and regulation of mitotic recombination in Saccharomyces cerevisiae. *Genetics*, **198**, 795-835.

18. Casari, E., Rinaldi, C., Marsella, A., Gnugnoli, M., Colombo, C.V., Bonetti, D. and Longhese, M.P. (2019) Processing of DNA Double-Strand Breaks by the MRX Complex in a Chromatin Context. *Front Mol Biosci*, **6**, 43.

19. Oh, J. and Symington, L.S. (2018) Role of the Mre11 Complex in Preserving Genome Integrity. *Genes (Basel)*, **9**.

20. Sasaki, M. and Kobayashi, T. (2017) Ctf4 Prevents Genome Rearrangements by Suppressing DNA Double-Strand Break Formation and Its End Resection at Arrested Replication Forks. *Molecular cell*, **66**, 533-545 e535.

21. Sasaki, M. and Kobayashi, T. (2023) Transcription near arrested DNA replication forks triggers ribosomal DNA copy number changes. *bioRxiv*, 2023.2012.2021.572944.

22. Kobayashi, T. and Ganley, A.R. (2005) Recombination regulation by transcription-induced cohesin dissociation in rDNA repeats. *Science*, **309**, 1581-1584.

23. Laloraya, S., Guacci, V. and Koshland, D. (2000) Chromosomal addresses of the cohesin component Mcd1p. *J Cell Biol*, **151**, 1047-1056.

24. Serra-Cardona, A. and Zhang, Z. (2018) Replication-Coupled Nucleosome Assembly in the Passage of Epigenetic Information and Cell Identity. *Trends Biochem Sci*, **43**, 136-148.

25. Stewart-Morgan, K.R., Petryk, N. and Groth, A. (2020) Chromatin replication and epigenetic cell memory. *Nat Cell Biol*, **22**, 361-371.

26. Driscoll, R., Hudson, A. and Jackson, S.P. (2007) Yeast Rtt109 promotes genome stability by acetylating histone H3 on lysine 56. *Science*, **315**, 649-652.

27. Masumoto, H., Hawke, D., Kobayashi, R. and Verreault, A. (2005) A role for cell-cycle-regulated histone H3 lysine 56 acetylation in the DNA damage response. *Nature*, **436**, 294-298.

28. Han, J., Zhou, H., Horazdovsky, B., Zhang, K., Xu, R.M. and Zhang, Z. (2007) Rtt109 acetylates histone H3 lysine 56 and functions in DNA replication. *Science*, **315**, 653-655.

29. Shibahara, K. and Stillman, B. (1999) Replication-dependent marking of DNA by PCNA facilitates CAF-1-coupled inheritance of chromatin. *Cell*, **96**, 575-585.

30. Smith, S. and Stillman, B. (1989) Purification and characterization of CAF-I, a human cell factor required for chromatin assembly during DNA replication in vitro. *Cell*, **58**, 15-25.

31. Zhang, Z., Shibahara, K. and Stillman, B. (2000) PCNA connects DNA replication to epigenetic inheritance in yeast. *Nature*, **408**, 221-225.

32. Enomoto, S. and Berman, J. (1998) Chromatin assembly factor I contributes to the maintenance, but not the re-establishment, of silencing at the yeast silent mating loci. *Genes Dev*, **12**, 219-232.

33. Kaufman, P.D., Kobayashi, R. and Stillman, B. (1997) Ultraviolet radiation sensitivity and reduction of telomeric silencing in Saccharomyces cerevisiae cells lacking chromatin assembly factor-I. *Genes Dev*, **11**, 345-357.

34. Smith, J.S., Caputo, E. and Boeke, J.D. (1999) A genetic screen for ribosomal DNA silencing defects identifies multiple DNA replication and chromatin-modulating factors. *Molecular and cellular biology*, **19**, 3184-3197.

35. Smith, D.J. and Whitehouse, I. (2012) Intrinsic coupling of lagging-strand synthesis to chromatin assembly. *Nature*, **483**, 434-438.

36. Borges, V., Smith, D.J., Whitehouse, I. and Uhlmann, F. (2013) An Eco1-independent sister chromatid cohesion establishment pathway in S. cerevisiae. *Chromosoma*, **122**, 121-134.

37. Yadav, T. and Whitehouse, I. (2016) Replication-Coupled Nucleosome Assembly and Positioning by ATP-Dependent Chromatin-Remodeling Enzymes. *Cell Rep*, **15**, 715-723.

38. Sasaki, M. and Kobayashi, T. (2021) Gel Electrophoresis Analysis of rDNA Instability in Saccharomyces cerevisiae. *Methods Mol Biol*, **2153**, 403-425.

39. Goto, M., Sasaki, M. and Kobayashi, T. (2021) The S-Phase Cyclin Clb5 Promotes rRNA Gene (rDNA) Stability by Maintaining Replication Initiation Efficiency in rDNA. *Molecular and cellular biology*, **41**.

40. Iida, T. and Kobayashi, T. (2019) RNA Polymerase I Activators Count and Adjust Ribosomal RNA Gene Copy Number. *Molecular cell*, **73**, 645-654 e613.

41. Saka, K., Takahashi, A., Sasaki, M. and Kobayashi, T. (2016) More than 10% of yeast genes are related to genome stability and influence cellular senescence via rDNA maintenance. *Nucleic Acids Res*.

42. Kaeberlein, M., McVey, M. and Guarente, L. (1999) The SIR2/3/4 complex and SIR2 alone promote longevity in Saccharomyces cerevisiae by two different mechanisms. *Genes Dev*, **13**, 2570-2580.

43. Krawitz, D.C., Kama, T. and Kaufman, P.D. (2002) Chromatin assembly factor I mutants defective for PCNA binding require Asf1/Hir proteins for silencing. *Molecular and cellular biology*, **22**, 614-625.

44. Ide, S. and Kobayashi, T. (2010) Analysis of DNA replication in Saccharomyces cerevisiae by two-dimensional and pulsed-field gel electrophoresis. *Curr Protoc Cell Biol*, **Chapter 22**, Unit 22 14.

45. Sauty, S.M. and Yankulov, K. (2023) Analyses of POL30 (PCNA) reveal positional effects in transient repression or bi-modal active/silent state at the sub-telomeres of S. cerevisiae. *Epigenetics Chromatin*, **16**, 40.

46. Hosoyamada, S., Sasaki, M. and Kobayashi, T. (2019) The CCR4-NOT Complex Maintains Stability and Transcription of rRNA Genes by Repressing Antisense Transcripts. *Molecular and cellular biology*, **40**.

47. Houseley, J., Kotovic, K., El Hage, A. and Tollervey, D. (2007) Trf4 targets ncRNAs from telomeric and rDNA spacer regions and functions in rDNA copy number control. *EMBO J*, **26**, 4996-5006.

48. Gruber, S., Arumugam, P., Katou, Y., Kuglitsch, D., Helmhart, W., Shirahige, K. and Nasmyth, K. (2006) Evidence that loading of cohesin onto chromosomes involves opening of its SMC hinge. *Cell*, **127**, 523-537.

49. Pakchuen, S., Ishibashi, M., Takakusagi, E., Shirahige, K. and Sutani, T. (2016) Physical Association of Saccharomyces cerevisiae Polo-like Kinase Cdc5 with Chromosomal Cohesin Facilitates DNA Damage Response. *The Journal of biological chemistry*, **291**, 17228-17246.

50. Sauer, P.V., Gu, Y., Liu, W.H., Mattiroli, F., Panne, D., Luger, K. and Churchill, M.E. (2018) Mechanistic insights into histone deposition and nucleosome assembly by the chromatin assembly factor-1. *Nucleic Acids Res*, **46**, 9907-9917.

51. Ghaddar, N., Luciano, P., Geli, V. and Corda, Y. (2023) Chromatin assembly factor-1 preserves genome stability in ctf4Delta cells by promoting sister chromatid cohesion. *Cell Stress*, **7**, 69-89.

52. Rouillon, C., Eckhardt, B.V., Kollenstart, L., Gruss, F., Verkennis, A.E.E., Rondeel, I., Krijger, P.H.L., Ricci, G., Biran, A., van Laar, T. *et al.* (2023) CAF-1 deposits newly synthesized histones during DNA replication using distinct mechanisms on the leading and lagging strands. *Nucleic Acids Res*, **51**, 3770-3792.

53. Ide, S., Saka, K. and Kobayashi, T. (2013) Rtt109 prevents hyper-amplification of ribosomal RNA genes through histone modification in budding yeast. *PLoS Genet*, **9**, e1003410.

FIGURE LEGENDS

Figure 1. CAF-1 is required for the maintenance of rDNA stability.

(A) Replication fork arrest, DSB formation and rDNA copy number changes in the budding yeast rDNA region. Chr XII carries the rDNA cluster, as indicated by the green bar. Each copy contains 35S rRNA (35S), 5S rRNA (5S), an origin of DNA replication (ARS), a cohesin-associated region (CAR), a cohesin-associated region (CAR), a bidirectional promoter for noncoding RNA, called E-pro, and a replication fork barrier (RFB). The black bar indicates the position of probe 1 used for ERC detection.

(B) PFGE analysis to examine the size heterogeneity of chr XII. DNA from independent clones of the indicated strains was separated by PFGE and stained with ethidium bromide. M indicates *Hansenula wingei* chromosomal DNA markers.

(C) ERC detection. DNA was isolated from the three indicated strains and separated by agarose gel electrophoresis, followed by Southern blotting with the probe 1, as shown in (A). Genomic rDNA and different forms of ERCs are indicated. M indicates lambda Hind III DNA markers. The top panel shows a short exposure of genomic rDNA signals.

(D) Quantitation of ERC levels. ERCs in (C) were quantified and their levels were compared between the WT and other mutants by one-way ANOVA, followed by Tukey's multiple comparisons test. Bars show mean ± s.e.m. Asterisks indicate statistically significant differences between WT and mutant strains ($p < 0.05$).

(E) Proportion of different forms of ERCs. In each sample, monomeric, dimeric and multimeric ERCs were quantified and the proportion of each form in total was determined. Under these conditions, supercoiled monomers are not detected.

Figure 2. Interaction with PCNA is necessary for CAF-1 to stabilize rDNA.

(A, D) PFGE analysis to examine the size heterogeneity of chr XII. DNA from independent clones of the indicated strains was separated by PFGE and stained with ethidium bromide. M indicates *Hansenula wingei* chromosomal DNA markers.

(B, E) ERC detection. DNA was isolated from the indicated strains and separated by agarose gel electrophoresis, followed by Southern blotting with the probe 1, as shown in Fig. 1A. Genomic rDNA and different forms of ERCs are indicated. M indicates lambda Hind III DNA markers. The top panel shows a short exposure of genomic rDNA signals.

(C, F) Quantitation of ERC levels. ERCs in (B, E) were quantified and their levels were normalized to those of the *cac1Δ* strain complemented with a plasmid carrying *CAC1* in (C) and the *pol30Δ* strain complemented with a plasmid carrying *POL30* in (F). ERC levels among different strains were compared by one-way ANOVA, followed by Tukey's multiple comparisons test. Bars show mean ± s.e.m. Asterisks above bars and above brackets indicate statistically significant differences between WT and mutant strains and between mutant strains, respectively ($p < 0.05$).

Figure 3. CAF-1 suppresses HR-mediated rDNA instability in response to Fob1-dependent replication fork arrest.

(A) PFGE analysis to examine the size heterogeneity of chr XII. DNA from independent clones of the indicated strains was separated by PFGE and stained with ethidium bromide. M indicates *Hansenula wingei* chromosomal DNA markers.

(B) ERC detection. DNA was isolated from the indicated strains and separated by agarose gel electrophoresis, followed by Southern blotting with the probe 1, as shown in Fig. 1A. Genomic rDNA and different forms of ERCs are indicated. M indicates lambda Hind III DNA markers. The top panel shows a short exposure of genomic rDNA signals. WT-1 was the same as to the first sample among the four WT clones that were analyzed on the left membrane.

(C) Quantitation of ERC levels. ERCs in (B, E) were quantified and their levels were compared between WT and other mutants by one-way ANOVA, followed by Tukey's multiple comparisons test. Bars show mean ± s.e.m. Asterisks above bars and above brackets indicate statistically significant differences between WT and mutant strains and between mutant strains, respectively ($p < 0.05$).

(D) The position of probe 1 used for 2D analysis. *N* indicates a site recognized by the restriction enzyme Nhe I.

(E) 2D agarose gel electrophoresis. Genomic DNA from the indicated strains was digested with Nhe I and separated by size in the first dimension and by size and shape in the second dimension, followed by Southern blotting with probe 1, as indicated in (D). The diagram on the top shows the expected migration pattern of different replication and recombination intermediates. 1N and 2N represent linear DNA and DNA fragments that are nearly completely replicated, respectively.

(F, G, H) Quantitation of replication and recombination intermediates. The signals of bubble arcs (F), arrested forks (G), and double Y and X molecules (H) were quantified relative to the total amount of replication and recombination intermediate signals. The levels of different molecules were determined in three independent samples of WT and *cac1Δ* and their levels were normalized to the average for WT. The levels of different molecules between WT and *cac1Δ* were compared by the two-sided Student's t-tests. Bars show mean ± s.e.m.; ns indicates that the difference was not statistically significant ($p > 0.05$).

Figure 4. CAF-1 affects transcription from E-pro.

(A) Positions of probes used for the detection of noncoding RNA by Northern blotting.

(B, D, F) Detection of noncoding RNAs transcribed from the intergenic regions in the rDNA. Total RNA was isolated from three independent clones of the indicated strains carrying the native E-pro in (B, D) and two independent clones of the indicated strains in the Gal-pro background grown either in the presence of raffinose or galactose in the media in (F). RNA was separated by size on formaldehyde-agarose and transcripts were analyzed by Northern blotting. In (B) and (F), IGS1-R was detected with probe 3 as indicated in (A). In (D), IGS1-F was detected with probe 4 as indicated in (A). The membranes were reprobed for *TSA1* transcripts as a control for loading.

(C, E, G) Quantitation of noncoding RNA. In (C) and (G), signals corresponding to IGS1-R transcripts in (C, G) were quantified relative to *TSA1*, which was normalized to the average of WT clones. In (F), IGS1-F transcripts were quantified relative to *TSA1*, which was normalized to the average of WT clones in the Gal-pro background grown in the presence of raffinose. Bars show mean ± s.e.m. in (C) and (E) and mean and the range from two independent experiments in (G). Transcript levels were compared by one-way ANOVA, followed by Tukey's multiple comparisons test in (C) and (E); *, statistically significant difference between WT and mutants ($p < 0.05$); ns, no significant difference ($p > 0.05$).

(H) ERC detection. DNA was isolated from the indicated strains in the Gal-pro background and separated by agarose gel electrophoresis, followed by Southern blotting with the probe 1, as shown in Fig. 1A. Genomic rDNA and different forms of ERCs are indicated. The sizes of lambda Hind III DNA markers are indicated. The top panel shows a short exposure of genomic rDNA signals.

(I) Quantitation of ERC levels. ERCs in three independent clones of the indicated strains, which included two clones, as shown in (H), and the third clone, which was analyzed on a different agarose gel, were quantified. ERC levels were compared between the WT and other mutants by one-way ANOVA, followed by Tukey's multiple comparisons test. Bars show mean ± s.e.m. Asterisks above bars and above brackets indicate statistically significant differences between WT and mutants and between mutants, respectively ($p < 0.05$).

Figure 5. CAF-1 suppresses DSB end resection.

(A, B, C) ChIP-qPCR analyses of Mcd1-Flag in the indicated strains. The regions where cohesin enrichments were examined are indicated as black bars. Four different regions in the rDNA region (i)–(iv) in (A), the positive control region near CEN6 in (B) and the negative control region near *YEL088W* on chr V (C) were examined. Untagged strains were used as controls. ChIP was performed using an antibody against a Flag epitope tag. The enrichment of chromatin in the indicated regions is expressed as the % input (IP/whole-cell extract). The bars show the means ± s.e.m. from three independent cultures of each strain.

(D) Restriction map and the positions of the probe 2 used for DSB analyses. The restriction sites for Bgl II (Bg) are indicated.

(E) DSB assay. Time-course experiments were conducted by arresting the indicated strains in the *GAL-FOB1* background in G1 with alpha factor, releasing the cells into fresh media and collecting the cells at different time points. Genomic DNA was isolated, digested with Bgl II, separated by size, and analyzed by Southern blotting with probe 2, as shown in (D). Arrested forks, linear fragments, DSBs and resected DSBs are indicated. Terminal fragments indicate the telomere-proximal rDNA repeat. Long exposure panels around DSBs and resected DSBs are shown below.

(F) Quantitation of DSBs. The frequency of DSBs was determined by quantifying the maximum signal of DSBs relative to the maximum signal of arrested forks in each time course. The average DSB frequency from three independent time course experiments was determined and normalized to the

average of WT clones (bars show mean ± s.e.m). Multiple comparisons were performed by one-way ANOVA, followed by Tukey's multiple comparisons test.

(G) Quantitation of resected DSBs. The frequency of resected DSB was determined by quantifying the maximum signal of resected DSBs relative to the maximum signal of DSBs in each time course. The average frequency of resected DSBs from three independent time course experiments was determined and normalized to the average of WT clones (bars show mean ± s.e.m). Multiple comparisons were performed by one-way ANOVA, followed by Tukey's multiple comparisons test; *, statistically significant difference ($p < 0.05$).

Figure 6. A model for CAF-1-mediated rDNA stabilization.

(A) The size of Okazaki fragments generated during rDNA replication. The WT and *cac1Δ* mutant carrying a doxycycline-repressible allele of *CDC9* were treated or not treated with doxycycline (Dox). Genomic DNA was isolated and separated on a denaturing agarose gel, followed by Southern blotting with a rDNA probe 1, as indicated in Fig. 1A. Profiles of the WT and *cac1Δ* strains, in which *CDC9* was shut off, were included. The positions of the bands of Okazaki fragments are indicated by arrowheads.

(B) A model for CAF-1-mediated rDNA stabilization. Left: CAF-1 facilitates nucleosome assembly onto replicating DNA by depositing a newly synthesized $(H3\text{-}H4)_2$ tetramer where H3K56 is acetylated (Ac). The assembly of the properly spaced nucleosome leads to the repression of transcription from E-pro. DSBs formed in this chromatin environment are repaired in a manner that does not involve rDNA copy number changes. Right: The absence of CAF-1 leads to defects in depositing newly synthesized histones. This environment results in the activation of transcription from E-pro, leading to the induction of DSB end resection and HR-mediated DSB repair. The HR protein Rad52 bound to resected DSBs preferentially uses the rDNA copy in a chromatin environment with histone H3K56Ac. Because the density of histone H3 acetylated at K56 is low in the CAF-1-defective strain, Rad52 assembled on the replicated DNA preferentially uses the distant rDNA copy, inducing rDNA instability.

Figure 1

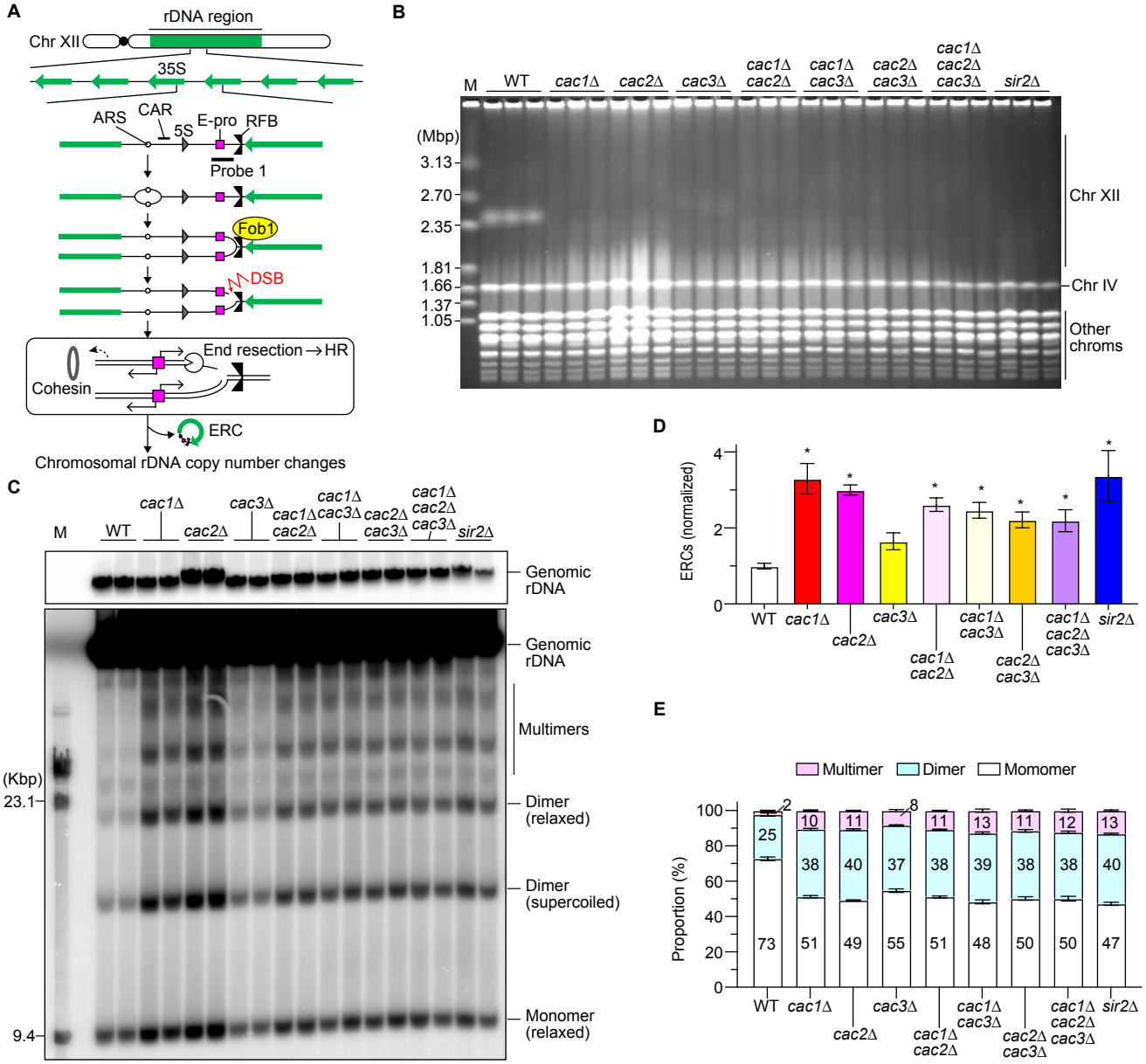

Figure 1. CAF-1 is required for the maintenance of rDNA stability.
(A) Replication fork arrest, DSB formation and rDNA copy number changes in the budding yeast rDNA region. Chr XII carries the rDNA cluster, as indicated by the green bar. Each copy contains 35S rRNA (35S), 5S rRNA (5S), an origin of DNA replication (ARS), a cohesin-associated region (CAR), a cohesin-associated region (CAR), a bidirectional promoter for noncoding RNA, called E-pro, and a replication fork barrier (RFB). The black bar indicates the position of probe 1 used for ERC detection.
(B) PFGE analysis to examine the size heterogeneity of chr XII. DNA from independent clones of the indicated strains was separated by PFGE and stained with ethidium bromide. M indicates Hansenula wingei chromosomal DNA markers.
(C) ERC detection. DNA was isolated from the three indicated strains and separated by agarose gel electrophoresis, followed by Southern blotting with the probe 1, as shown in (A). Genomic rDNA and different forms of ERCs are indicated. M indicates lambda Hind III DNA markers. The top panel shows a short exposure of genomic rDNA signals.
(D) Quantitation of ERC levels. ERCs in (C) were quantified and their levels were compared between the WT and other mutants by one-way ANOVA, followed by Tukey's multiple comparisons test. Bars show mean ± s.e.m. Asterisks indicate statistically significant differences between WT and mutant strains ($p < 0.05$).
(E) Proportion of different forms of ERCs. In each sample, monomeric, dimeric and multimeric ERCs were quantified and the proportion of each form in total was determined. Under these conditions, supercoiled monomers are not detected.

Figure 2

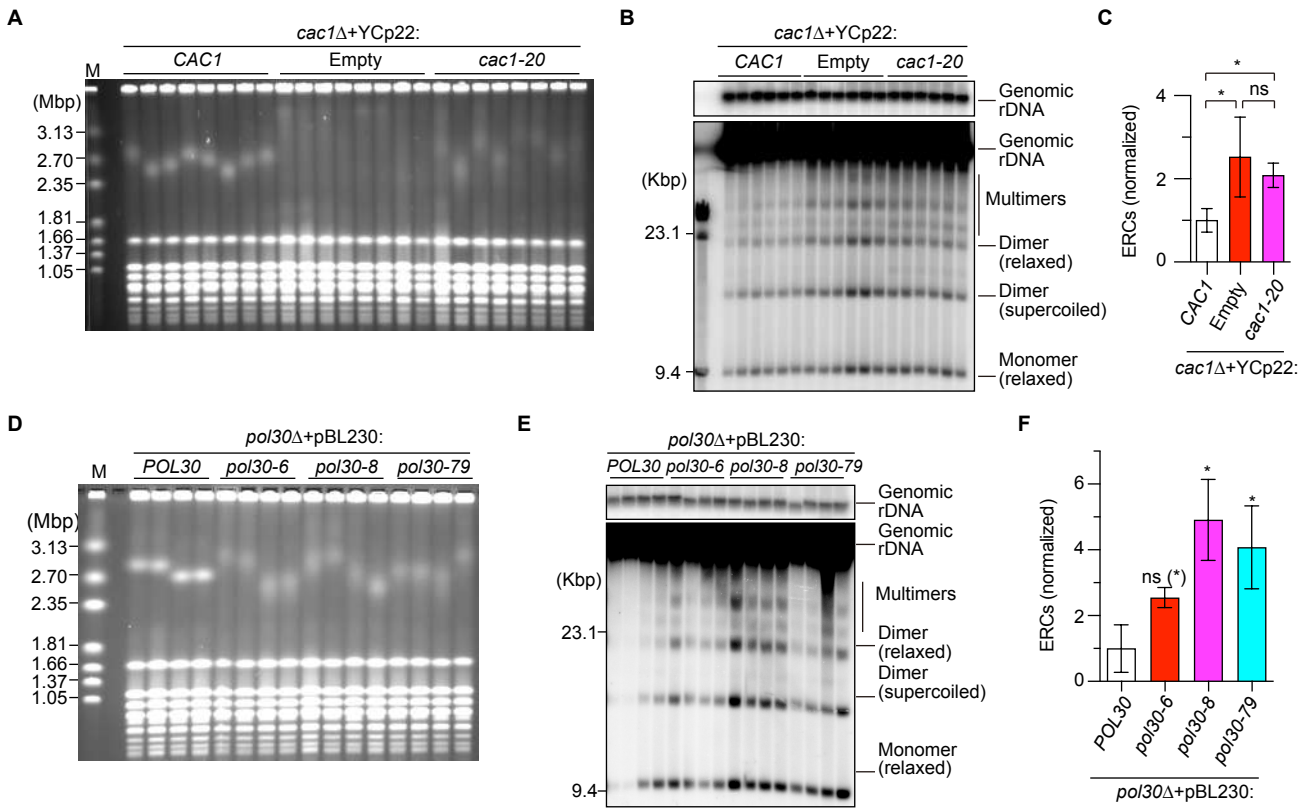

Figure 2. Interaction with PCNA is necessary for CAF-1 to stabilize rDNA.
(A, D) PFGE analysis to examine the size heterogeneity of chr XII. DNA from independent clones of the indicated strains was separated by PFGE and stained with ethidium bromide. M indicates Hansenula wingei chromosomal DNA markers.
(B, E) ERC detection. DNA was isolated from the indicated strains and separated by agarose gel electrophoresis, followed by Southern blotting with the probe 1, as shown in Fig. 1A. Genomic rDNA and different forms of ERCs are indicated. M indicates lambda Hind III DNA markers. The top panel shows a short exposure of genomic rDNA signals.
(C, F) Quantitation of ERC levels. ERCs in (B, E) were quantified and their levels were normalized to those of the cac1Δ strain complemented with a plasmid carrying CAC1 in (C) and the pol30Δ strain complemented with a plasmid carrying POL30 in (F). ERC levels among different strains were compared by one-way ANOVA, followed by Tukey's multiple comparisons test. Bars show mean ± s.e.m. Asterisks above bars and above brackets indicate statistically significant differences between WT and mutant strains and between mutant strains, respectively ($p < 0.05$).

Figure 3

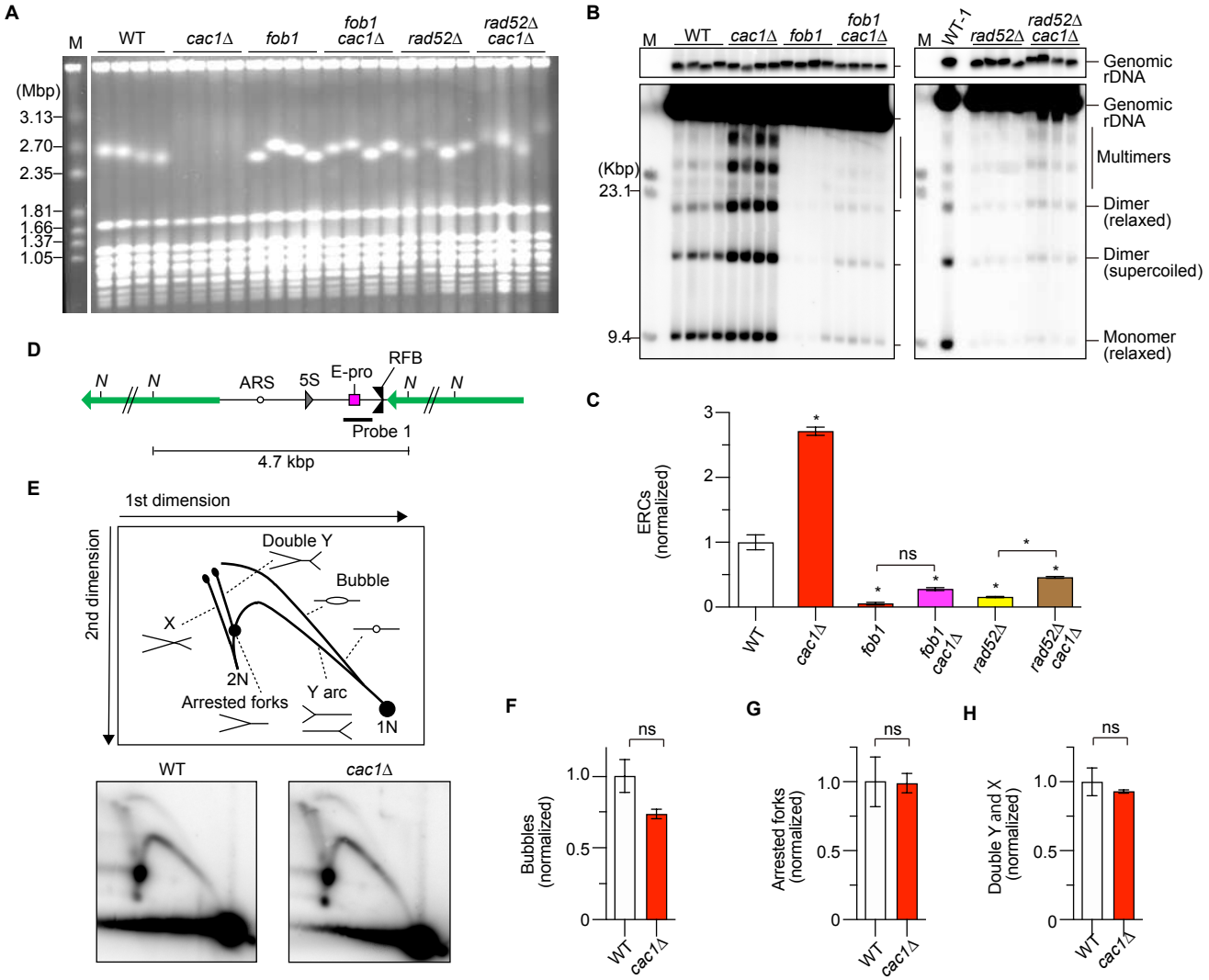

Figure 3. CAF-1 suppresses HR-mediated rDNA instability in response to Fob1-dependent replication fork arrest.
(A) PFGE analysis to examine the size heterogeneity of chr XII. DNA from independent clones of the indicated strains was separated by PFGE and stained with ethidium bromide. M indicates Hansenula wingei chromosomal DNA markers.
(B) ERC detection. DNA was isolated from the indicated strains and separated by agarose gel electrophoresis, followed by Southern blotting with the probe 1, as shown in Fig. 1A. Genomic rDNA and different forms of ERCs are indicated. M indicates lambda Hind III DNA markers. The top panel shows a short exposure of genomic rDNA signals. WT-1 was the same as to the first sample among the four WT clones that were analyzed on the left membrane.
(C) Quantitation of ERC levels. ERCs in (B, E) were quantified and their levels were compared between WT and other mutants by one-way ANOVA, followed by Tukey's multiple comparisons test. Bars show mean ± s.e.m. Asterisks above bars and above brackets indicate statistically significant differences between WT and mutant strains and between mutant strains, respectively ($p < 0.05$).
(D) The position of probe 1 used for 2D analysis. N indicates a site recognized by the restriction enzyme Nhe I.
(E) 2D agarose gel electrophoresis. Genomic DNA from the indicated strains was digested with Nhe I and separated by size in the first dimension and by size and shape in the second dimension, followed by Southern blotting with probe 1, as indicated in (D). The diagram on the top shows the expected migration pattern of different replication and recombination intermediates. 1N and 2N represent linear DNA and DNA fragments that are nearly completely replicated, respectively.
(F, G, H) Quantitation of replication and recombination intermediates. The signals of bubble arcs (F), arrested forks (G), and double Y and X molecules (H) were quantified relative to the total amount of replication and recombination intermediate signals. The levels of different molecules were determined in three independent samples of WT and cac1Δ and their levels were normalized to the average for WT. The levels of different molecules between WT and cac1Δ were compared by the two-sided Student's t-tests. Bars show mean ± s.e.m.; ns indicates that the difference was not statistically significant ($p > 0.05$).

Figure 4

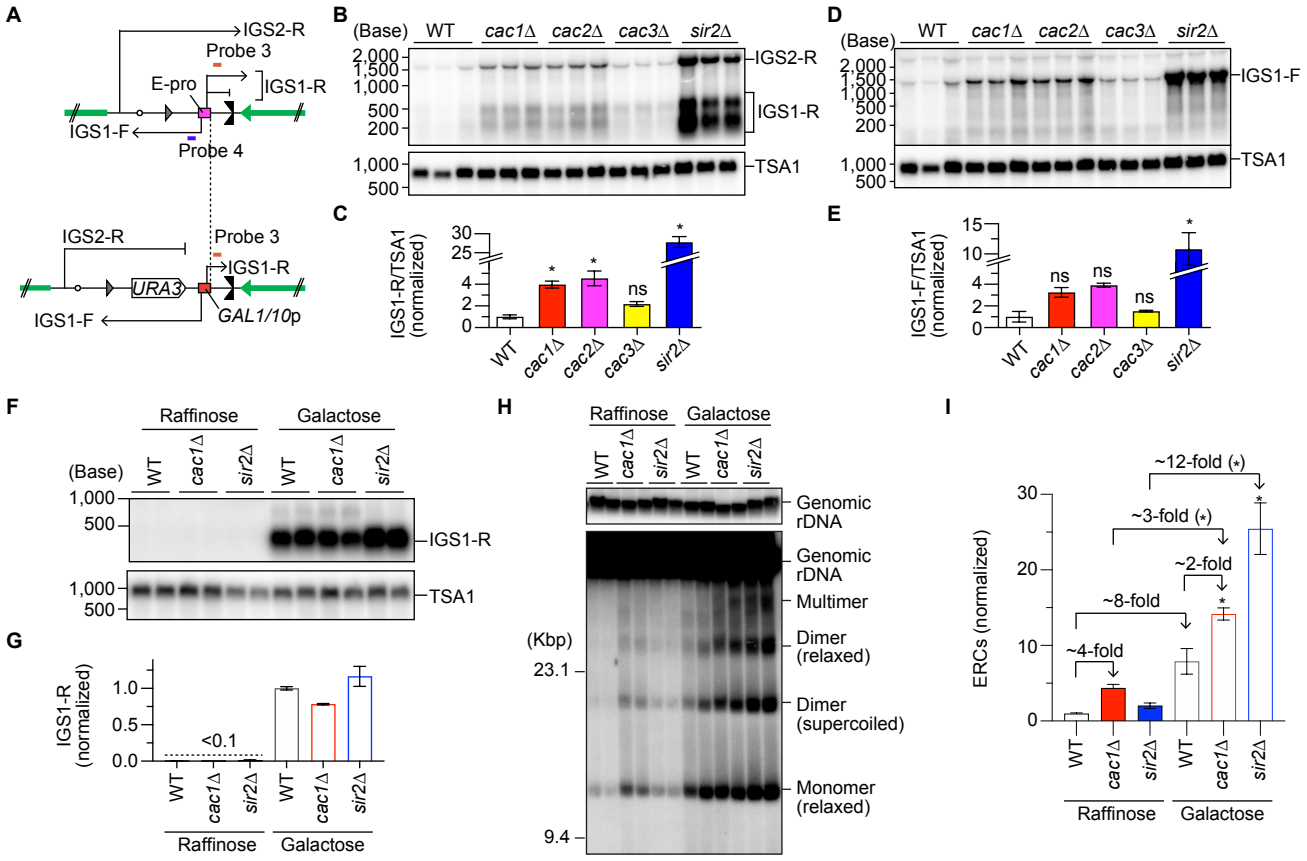

Figure 4. CAF-1 affects transcription from E-pro.
(A) Positions of probes used for the detection of noncoding RNA by Northern blotting.
(B, D, F) Detection of noncoding RNAs transcribed from the intergenic regions in the rDNA. Total RNA was isolated from three independent clones of the indicated strains carrying the native E-pro in (B, D) and two independent clones of the indicated strains in the Gal-pro background grown either in the presence of raffinose or galactose in the media in (F). RNA was separated by size on formaldehyde-agarose and transcripts were analyzed by Northern blotting. In (B) and (F), IGS1-R was detected with probe 3 as indicated in (A). In (D), IGS1-F was detected with probe 4 as indicated in (A). The membranes were reprobed for TSA1 transcripts as a control for loading.
(C, E, G) Quantitation of noncoding RNA. In (C) and (G), signals corresponding to IGS1-R transcripts in (C, G) were quantified relative to TSA1, which was normalized to the average of WT clones. In (F), IGS1-F transcripts were quantified relative to TSA1, which was normalized to the average of WT clones in the Gal-pro background grown in the presence of raffinose. Bars show mean ± s.e.m. in (C) and (E) and mean and the range from two independent experiments in (G). Transcript levels were compared by one-way ANOVA, followed by Tukey's multiple comparisons test in (C) and (E); *, statistically significant difference between WT and mutants ($p < 0.05$); ns, no significant difference ($p > 0.05$).
(H) ERC detection. DNA was isolated from the indicated strains in the Gal-pro background and separated by agarose gel electrophoresis, followed by Southern blotting with the probe 1, as shown in Fig. 1A. Genomic rDNA and different forms of ERCs are indicated. The sizes of lambda Hind III DNA markers are indicated. The top panel shows a short exposure of genomic rDNA signals.
(I) Quantitation of ERC levels. ERCs in three independent clones of the indicated strains, which included two clones, as shown in (H), and the third clone, which was analyzed on a different agarose gel, were quantified. ERC levels were compared between the WT and other mutants by one-way ANOVA, followed by Tukey's multiple comparisons test. Bars show mean ± s.e.m. Asterisks above bars and above brackets indicate statistically significant differences between WT and mutants and between mutants, respectively ($p < 0.05$).

Figure 5

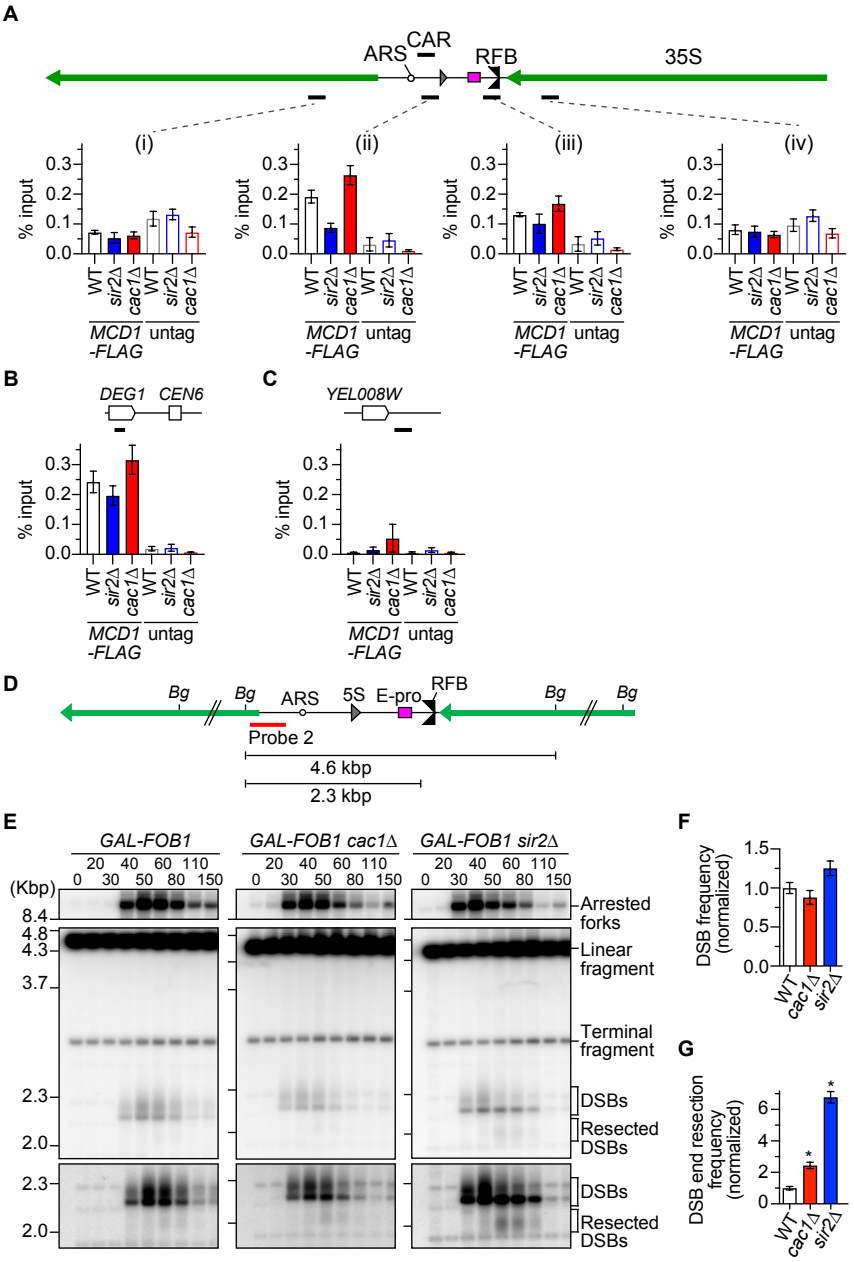

Figure 5. CAF-1 suppresses DSB end resection.
(A, B, C) ChIP–qPCR analyses of Mcd1-Flag in the indicated strains. The regions where cohesin enrichments were examined are indicated as black bars. Four different regions in the rDNA region (i)–(iv) in (A), the positive control region near CEN6 in (B) and the negative control region near YEL088W on chr V (C) were examined. Untagged strains were used as controls. ChIP was performed using an antibody against a Flag epitope tag. The enrichment of chromatin in the indicated regions is expressed as the % input (IP/whole-cell extract). The bars show the means ± s.e.m. from three independent cultures of each strain.
(D) Restriction map and the positions of the probe 2 used for DSB analyses. The restriction sites for Bgl II (Bg) are indicated.
(E) DSB assay. Time-course experiments were conducted by arresting the indicated strains in the GAL-FOB1 background in G1 with alpha factor, releasing the cells into fresh media and collecting the cells at different time points. Genomic DNA was isolated, digested with Bgl II, separated by size, and analyzed by Southern blotting with probe 2, as shown in (D). Arrested forks, linear fragments, DSBs and resected DSBs are indicated. Terminal fragments indicate the telomere-proximal rDNA repeat. Long exposure panels around DSBs and resected DSBs are shown below.
(F) Quantitation of DSBs. The frequency of DSBs was determined by quantifying the maximum signal of DSBs relative to the maximum signal of arrested forks in each time course. The average DSB frequency from three independent time course experiments was determined and normalized to the average of WT clones (bars show mean ± s.e.m). Multiple comparisons were performed by one-way ANOVA, followed by Tukey's multiple comparisons test.
(G) Quantitation of resected DSBs. The frequency of resected DSB was determined by quantifying the maximum signal of resected DSBs relative to the maximum signal of DSBs in each time course. The average frequency of resected DSBs from three independent time course experiments was determined and normalized to the average of WT clones (bars show mean ± s.e.m). Multiple comparisons were performed by one-way ANOVA, followed by Tukey's multiple comparisons test; *, statistically significant difference ($p < 0.05$).

Figure 6

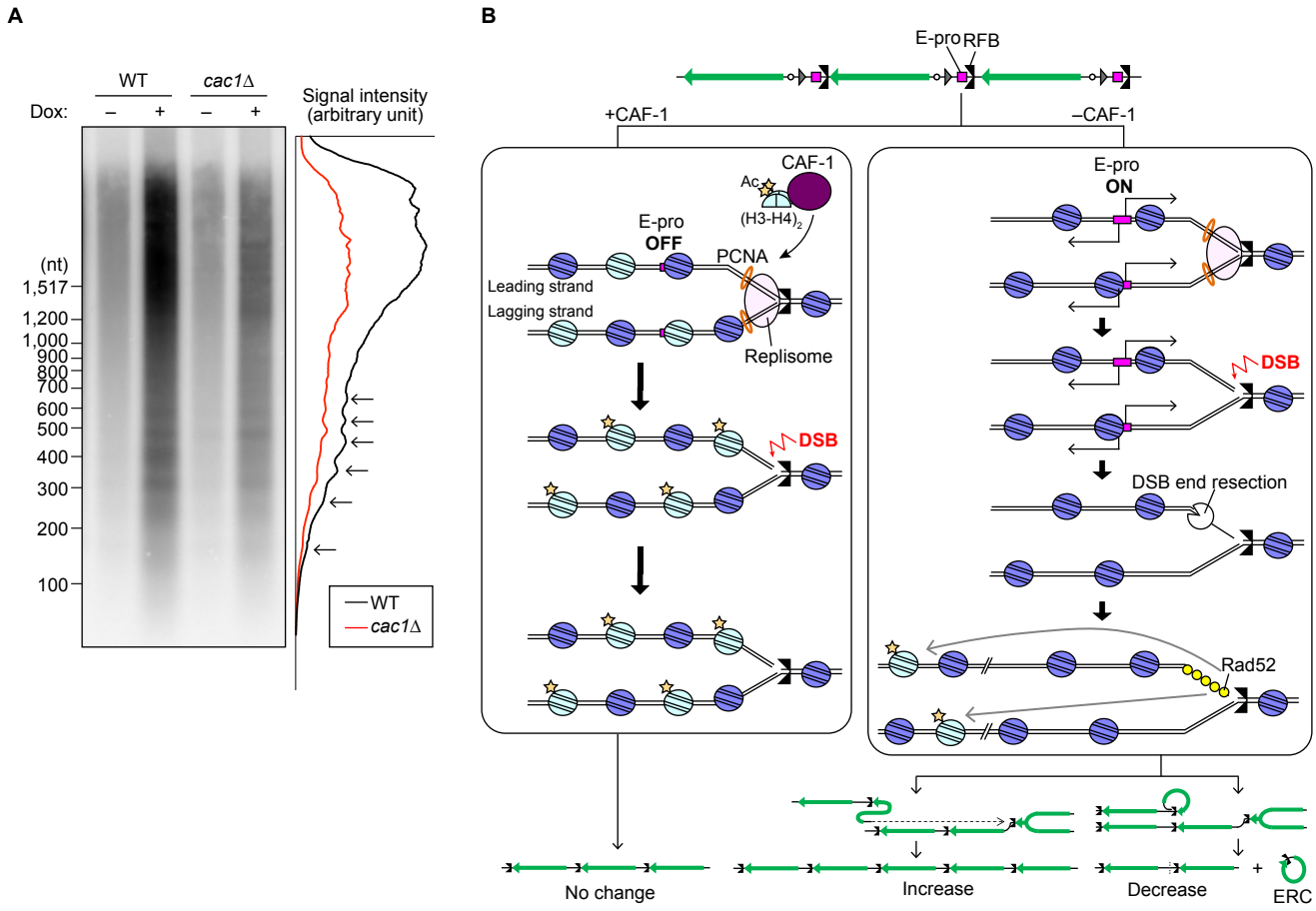

Figure 6. A model for CAF-1-mediated rDNA stabilization.
(A) The size of Okazaki fragments generated during rDNA replication. The WT and cac1Δ mutant carrying a doxycycline-repressible allele of CDC9 were treated or not treated with doxycycline (Dox). Genomic DNA was isolated and separated on a denaturing agarose gel, followed by Southern blotting with a rDNA probe 1, as indicated in Fig. 1A. Profiles of the WT and cac1Δ strains, in which CDC9 was shut off, were included. The positions of the bands of Okazaki fragments are indicated by arrowheads.
(B) A model for CAF-1-mediated rDNA stabilization. Left: CAF-1 facilitates nucleosome assembly onto replicating DNA by depositing a newly synthesized (H3-H4)2 tetramer where H3K56 is acetylated (Ac). The assembly of the properly spaced nucleosome leads to the repression of transcription from E-pro. DSBs formed in this chromatin environment are repaired in a manner that does not involve rDNA copy number changes. Right: The absence of CAF-1 leads to defects in depositing newly synthesized histones. This environment results in the activation of transcription from E-pro, leading to the induction of DSB end resection and HR-mediated DSB repair. The HR protein Rad52 bound to resected DSBs preferentially uses the rDNA copy in a chromatin environment with histone H3K56Ac. Because the density of histone H3 acetylated at K56 is low in the CAF-1-defective strain, Rad52 assembled on the replicated DNA preferentially uses the distant rDNA copy, inducing rDNA instability.